The Hebrew University of Jerusalem
Faculty of Mathematics and Sciences
Selim and Rachel Benin School of Engineering
Applied Physics Department

N×M Wavelength Selective Switch (WSS)

N×M מתג אופטי על בסיס אורך גל

by

Leonid Pascar

This work was done under the supervision of

Prof. Dan M. Marom

Thesis submitted for M.Sc. degree

December, 2014

This work is dedicated to my parents Abraham and Bella

Acknowledgments

I thank my father Abraham for encouraging me for studying and broadening my horizons in Physics.

I thank my mother Bella and my brother Gregory for supporting me throughout my life.

I thank my advisor Prof. Dan Marom for the guidance and advices that enabled me to carry out this project.

I would like to thank especially Reuven Karoubi, who taught me a lot about optics and helped me throughout the project.

I thank Boris Frenkel for his many advices that helped me a lot.

I thank David Sinefeld for his guidance when I was a new lab student.

I thank Dror Shayovich for his endless patience and many useful advices.

I thank Roy Rudnick for one good advice in a crucial moment

Abstract
A novel approach for a multi-port Wavelength Selective Switch (WSS) is shown in this work. The switching is performed from a series of 8 input fibers to a series of 24 output fibers. This device can be useful in reducing the complexity of optical communication nodes based on conventional switch with only one input fiber

The multi-port switching is based on a spatial separation, of light beams, according to input port and wavelength channel on a dynamic steering device – LCoS (Liquid Crystal on Silicon) SLM (Spatial light modulator).

The LCoS SLM was extensively characterized in order to understand the capabilities and limitations for better system design.

The system design is extensively discussed in this paper and a proof of concept experiment demonstrates that indeed this concept can be realized.

תקציר
בעבודה זו מוצג רעיון חדשני עבור מתג אופטי עם מספר סיבי כניסה ויצאה שהמיתוג בו מתבצע על בסיס אורך גל. אנו מציגים מכשיר בו ישנם שמונה סיבי כניסה ועשרים וארבעה סיבי יצירה. רכיב זה יכול לסייע בהורדת הסיבוכיות של צמתי התקשורת האופטית המבוססים כיום על מתגים בעלי סיב כניסה יחיד.

המיתוג ברכיב זה מתבסס על הפרדה לפי סיב כניסה ולפי ערוץ אורך גל על רכיב מאפנן פאזה שמאפשר הטיה זוויתית דינמית.

התכנון והשיקולים ההנדסיים נידונים בהרחבה בעבודה זו, כמו מוכן מוצגים תוצאות של ניסוי הוכחת היתכנות המראה שהמכשיר אכן ניתן ליישום.

Table of Contents

1. Introduction

1.1 "Black box" description.

The goal of *8×24* WSS is to redirect selected spectral components from a series of eight input fiber ports to a series of 24 output fiber ports. A "black box" scheme is shown in fig 1.1.1, in which 8 data ports with spectral channels $\lambda_1 ... \lambda_k$ (DWM signals) enter through the system's 8 input ports and are redirected to the output ports. There is one restriction regarding the switching possibilities: **Each output port can get data from only one input port at a time. This input port can be anyone out of the input array elements.**

Another option for multi input port switch is the Wavelength Selective Cross Connect (WSXC) [1] which routes DWM signals from N input fibers to N output fibers (short description of *10×10* WSXC, that we designed, can be found in Appendix B) as it is shown in figure 1.1.2. Wavelength channels from different input port can be directed to the same output port (unlike the 8×24 WSS). However, the WSXC suffers from major drawback of sensitivity to failures (discussed in appendix B).

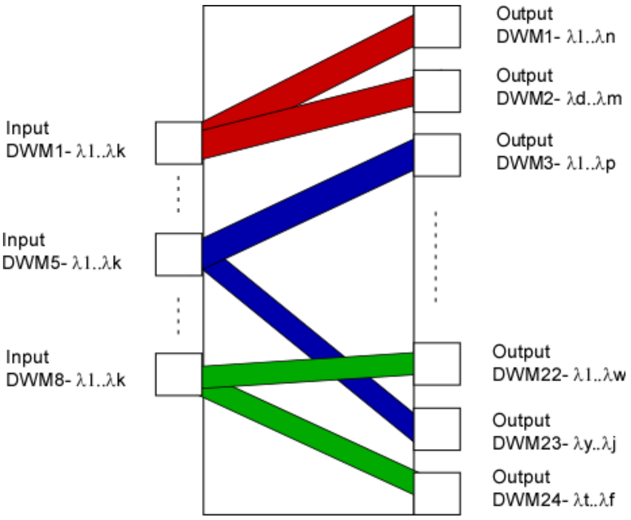

Fig. 1.1.1. An example of multi-port switching. The signals are steered from the input to the desired output ports. Each color represents an input port. Right: Several spectral channels (from different input ports) are routed to a single output port.

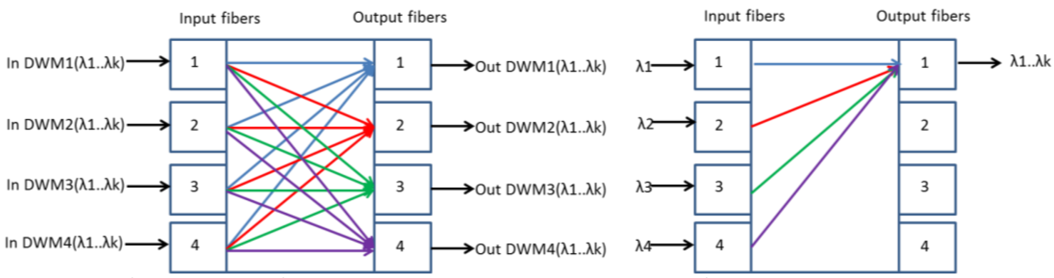

Fig. 1.1.2. Left: An example of multi-port switching. The signals are steered from the input to the desired output ports. Each color represents a target output port. Right: Several spectral channels (from different input ports) are routed to a single output port.

The system (*8×24* WSS) is based on a diffraction grating to separate different spectral components of each fiber port, where the routing is based on beam steering with a spatial light modulator (SLM) which is placed in the spectral plane, controlling the direction of the outgoing light beams

1.2 Importance of 8×24 WSS in a communication network

Optical switch is an important device in Reconfigurable Optical Add and Drop (ROADM) node. Firstly, the functionality of such node is discussed and later the current switching technology and ROADM architecture will be described in order to understand the necessity of 8×24 WSS.

1.2.1 ROADM node

The traffic of DWM signals, in the optical communication network, is controlled by multiple ROADM nodes[1] . The DWM signals are manipulated in each node, some spectral channels are "dropped" (thus, transferred to the receivers of the local data center), while others are routed to different nodes of the network.

The nodes support also the "add" operation, in which transmitted data channels are combined with existing WDM signals.

The modern ROADM nodes are required to be Colorless, Directionless and Contentionless (CDC) [2].

Colorless: Every wavelength can be assigned to any port at add/drop completely by software control without rewiring by technicians.

Directionless: Every wavelength can be routed to any direction served by the node completely by software control without rewiring by technician.

Contentionless: Multiple signals, with the same wavelength, can be routed on a single add/drop structure

The WDM channel are routed on wavelength basis, the current technology, which enables this operation, is the 1×k WSS.

1.2.2 1×k WSS

The 1×k WSS [3] is a device used for switching the spectral elements of a single DWM signal (from one input fiber) to multiple output ports as shown in fig 1.2.2.1

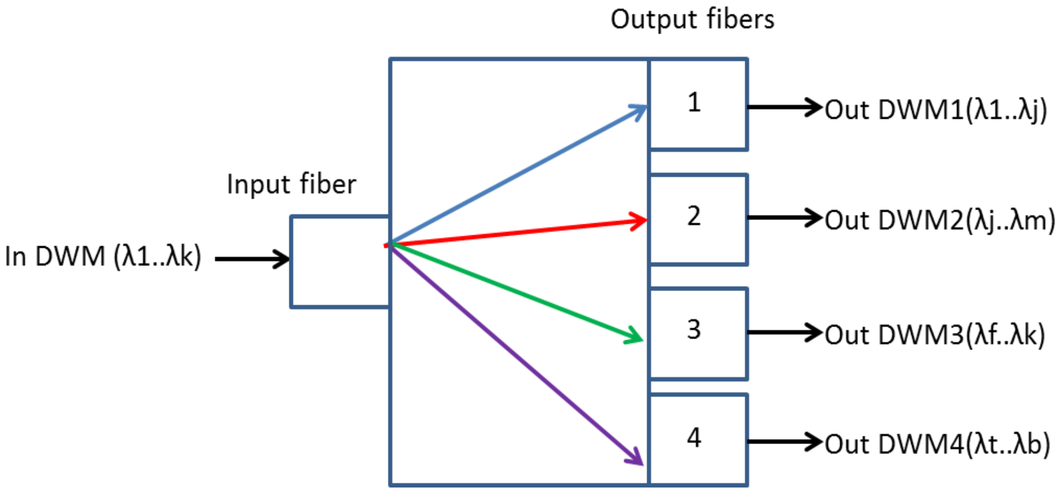

Fig. 1.2.2.1 Black box description of 1×k WSS

The spectral elements can be routed to any output port according to the desired switching configuration. It is important to emphasize that the 1×k WSS can be used in reverse for combining multiple spectral elements into one WDM signal.

The "add/drop" and routing operations, in a ROADM node, are performed by several 1×k WSS devices. Examples of 1×k WSS based network and ROADM nodes are shown in fig 1.2.2.2 and fig 1.2.2.3 respectively

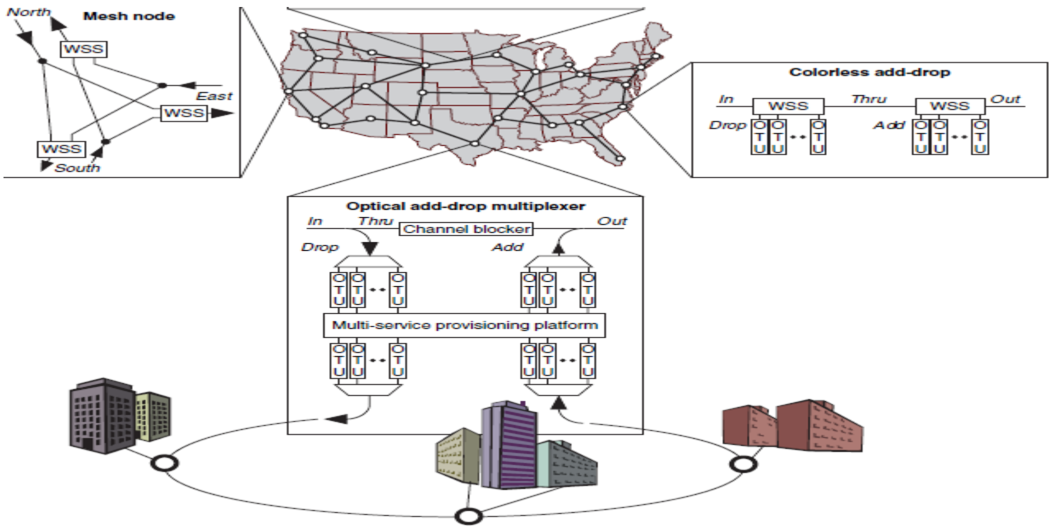

Fig. 1.2.2.2 1×k WSS based network

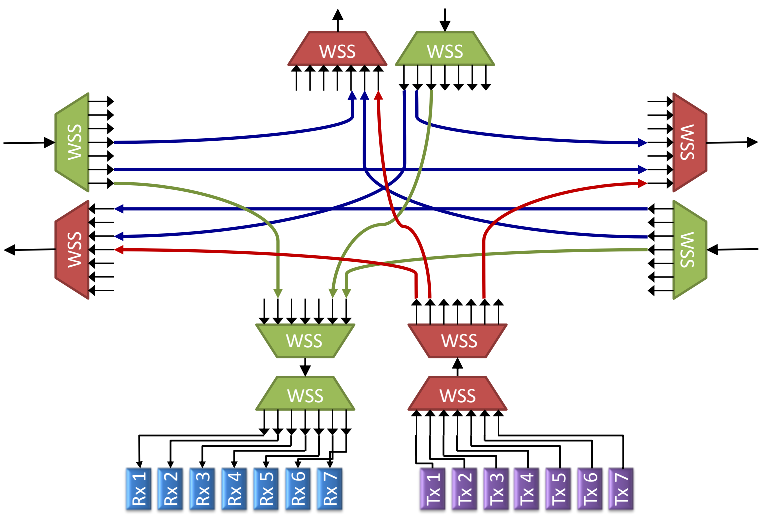

Fig. 1.2.2.3 1×k WSS based ROADM node

The architecture displayed in figure 1.2.2.3 suffers from contention as only one single per wavelength channel can be added or dropped by the WSS. It is possible to add more WSS devices, receivers and transmitters but it will lead to great complexity which does not meet the growing demands. Another architecture, which incorporates 1×k WSS with splitters and couplers (and amplifiers for power loss compensation), is the multi-cast switch [2] based ROADM (fig 1.2.2.4). This technology meets the CDC requirements. However, this system is complicated and costly.

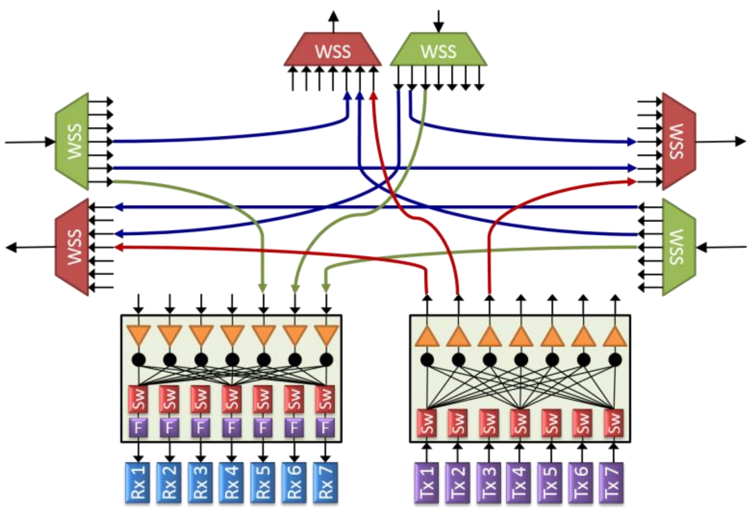

Fig. 1.2.2.4 Multi-cast switch based ROADM CDC

The spectral channel spacing, within a DWM signal, is becoming increasingly low. Which causes the ROADM nodes (in the current WSS technology) to become very complicated as many additional WSS devices are required in the node.

The current switching technology does not allow easy scalability for meeting the growing dense spectral channels demand. Another great disadvantage, of nodes with too many WSS devices, is the power losses (as every device adds loss). Multiple amplifiers are used for compensating it, but this leads to further complexity of the system as additional elements are added. Therefore, a high order switch (multiple input ports) will allow greater scalability and less loss will be inflicted (and number of amplifiers will be reduced)

ROADM node architecture, which incorporates 8×24 WSS, is shown in fig 1.2.2.5

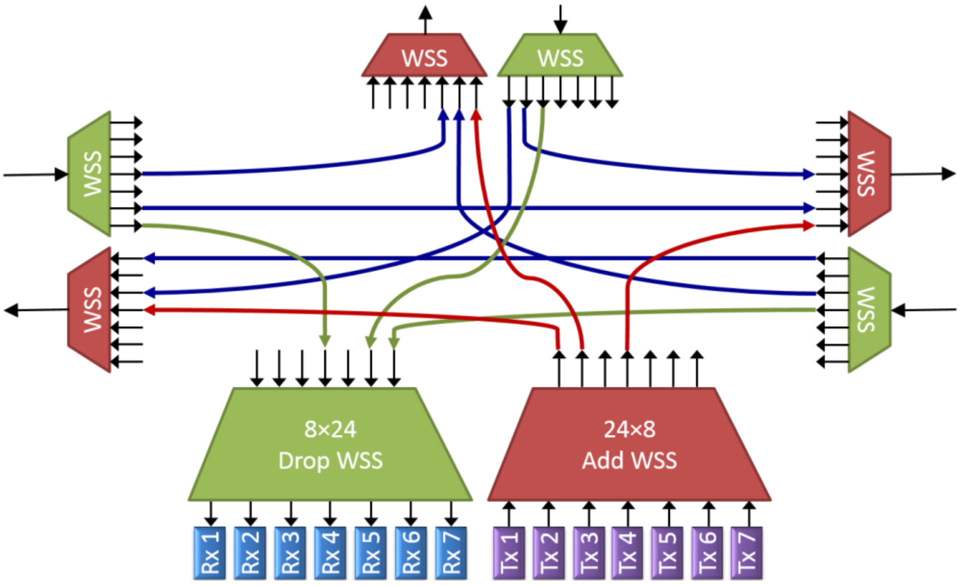

Fig. 1.2.2.5 8×24 WSS based ROADM node

1.3 Optical concept

This work is based on switching technology of the conventional 1×k WSS with modifications which allow high order switching that is required for meeting the growing spectral demands of the ROADM nodes.

The optical data signals are separated according to spectral channel and input port on the LCoS SLM, a dynamic steering element.

The spectral/port separation is achieved by using passive and active elements such as diffraction grating and MEMS micro mirror array.

The basic structure of conventional WSS is shown in figure 1.3.1. One DWM light beam is incident on a diffraction grating, which angularly disperses the light. The Fourier lens transforms the angular dispersion into a spatial dispersion on the switching element (LCoS SLM), which is positioned in the back Fourier plane.

The spatial separation of spectral channels is utilized for applying unique steering angle per wavelength channel. The Fourier lens transforms the steering angle to a spatial translation. This enables independent switching per DWM channel. However, this architecture does not support multi-port input and multi-port output switching.

We introduce also port separation which is achieved by MEMS micro mirrors array (detailed explanation in section 2 and 1.4.2).

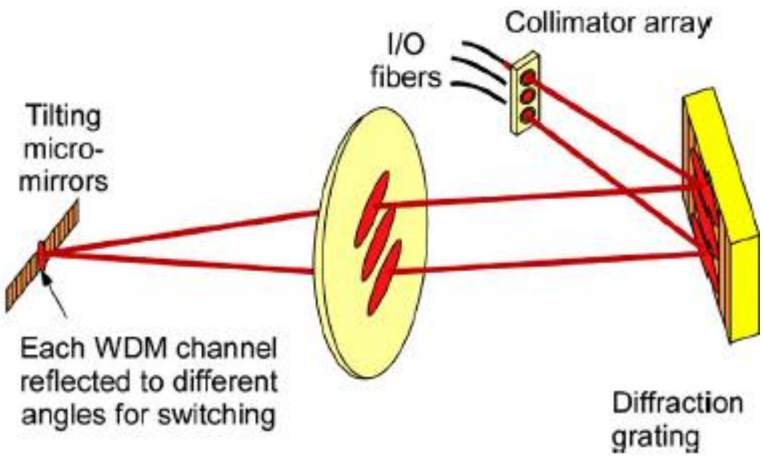

Fig. 1.3.1 Conventional WSS scheme.

1.4 Dynamic steering elements

There are two kinds of dynamic steering elements in this design: LCoS SLM and MEMS micro mirrors. Short description, of those devices, is given in the current section

1.4.1 Liquid Crystal on Silicon (LCoS) SLM

The LCoS SLM is a phase modulator (comprised of 2D pixels) based on alignment of liquid crystal molecules controlled by a voltage matrix supplied by a VLSI die. There are several liquid crystal phases. The LCoS SLM is based on Nematic phase Liquid Crystal.

Nematic phase: There is not a positional order but the molecules tend to point in the same direction. There are two forms of the Nematic phase which are used for modulators: Non-twisted and twisted.

The macroscopic direction does not vary along the sample in the non-twisted Nematic phase. Whereas, the orientation of molecules varies along the sample (fig 1.4.1.1) in the twisted Nematic phase.

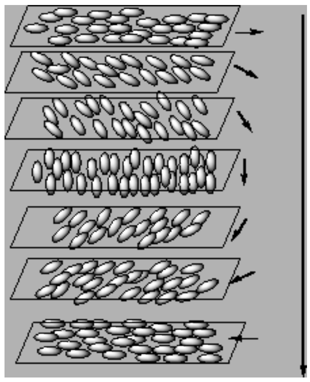

Fig. 1.4.1.1: Twisted Nematic. The macroscopic orientation varies along the sample.

The phase LCoS SLM (which we use in the design) is based on non-twisted Nematic liquid crystal. There are amplitude modulators which are based on the twisted Nematic liquid crystal [4]. We will treat only the non-twisted Nemtic phase.

Each pixel is a liquid crystal cell and its phase value is determined by the orientation of the liquid crystal molecules (fig 1.4.1.2). The angular orientation (θ) is dependent on the applied voltage (v) according to $\theta = \frac{\pi}{2} - 2\arctan(e^{-v})$ [4]. The rotation of the molecules affects the index ellipsoid according to $\frac{1}{n(\theta)^2} = \frac{\cos^2(\theta)}{n_0^2} + \frac{\sin^2(\theta)}{n_e^2}$ [5] where $n_{0,}$ n_e are the index of refraction of ordinary and extra ordinary axis respectively. Therefore, the phase retardation (ϕ) that each pixel apply is given by $\phi = \frac{2\pi}{\lambda}(n(v) - n_0)$.

The ability to determine the phase of each pixel in the matrix (fig 1.4.1.2) enables the user to apply diverse and complex phase patterns that can perform variety of operations such as beam deflection, adding wave-front curvature, spatial filtering, aberration compensation and more.

This device is utilized in our system for the purpose of beam steering

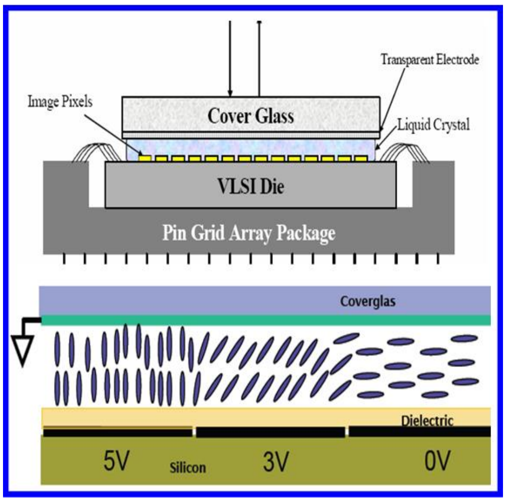

Fig. 1.4.1.2: LCoS physical layout

We use the Holoeye LCoS SLM in our system. Its specifications are listed below:

1) Pixel size (length and width) is 8μm.
2) The matrix pixel size is 1920×1080 (HD resolution)
3) The device is polarization sensitive.
4) The fill factor value is > 87%.
5) The applied phase values are between 0 and 2π
6) Insertion loss: 1-2dB (depends on the specific model)

1.4.2 Micro Electro-Mechanical Systems (MEMS) mirrors

The MEMS phase modulator [1] is based on pixelated mirror which tilt the beam. An actuator drives the mirror according to voltage applied by the CMOS electronic driver (fig 1.4.2.1)

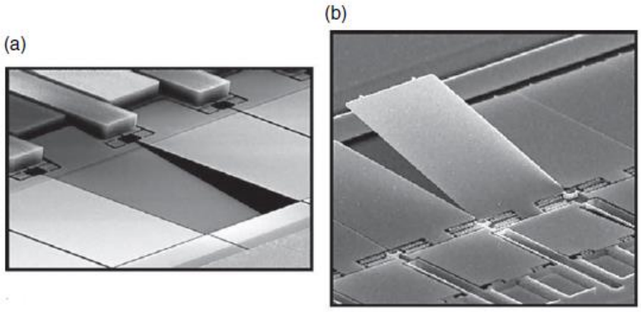

Fig. 1.4.2.1: MEMS modulator

The MEMS is utilized in our system for the purpose of beam steering, which creates (with the lens Fourier lens) spatial separation according to input channel on the LCoS SLM.

Unlike the LCoS SLM, the MEMS is polarization insensitive. However, the resolution of this device is limited compared to the LCoS SLM. Therefore, LCoS SLM is favored for performing the spectral switching.

2. System design

The design and the principle of operation of the 8×24 WSS will be extensively discussed in this part. The multi-port spectral switching is achieved by creating a spatial separation on the LCoS SLM according to input port and wavelength channel.

The 8×24 WSS is comprised of 3 conceptual sub parts (fig 2.1):

1) Input part-The light beams are spatially separated according to input port and spectral channel on the LCoS SLM.
2) Switching part: A tilt (which determines the switching) is applied on each light beam, by the LCoS SLM, according to desired switching configuration.
3) Output part: The light beams are routed to the desired output ports.

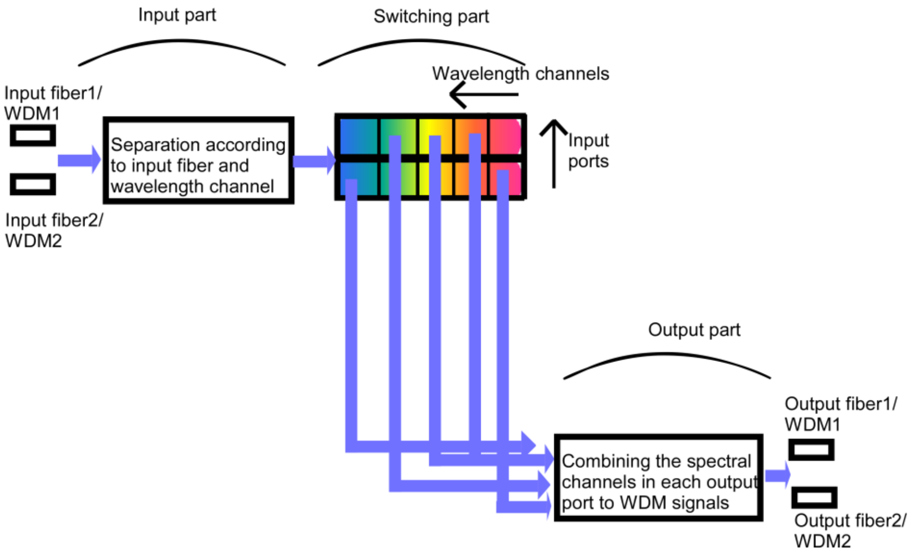

Fig. 2. 1: Conceptual structure of the device.

It is important to emphasize that same optical elements are used for the input and output parts. System is symmetric.

2.1 Input part

The light beams are separated according to input port and spectral channel, in this part, on the LCoS SLM plane (fig 2.1.1). This separation enables switching from multiple input ports.

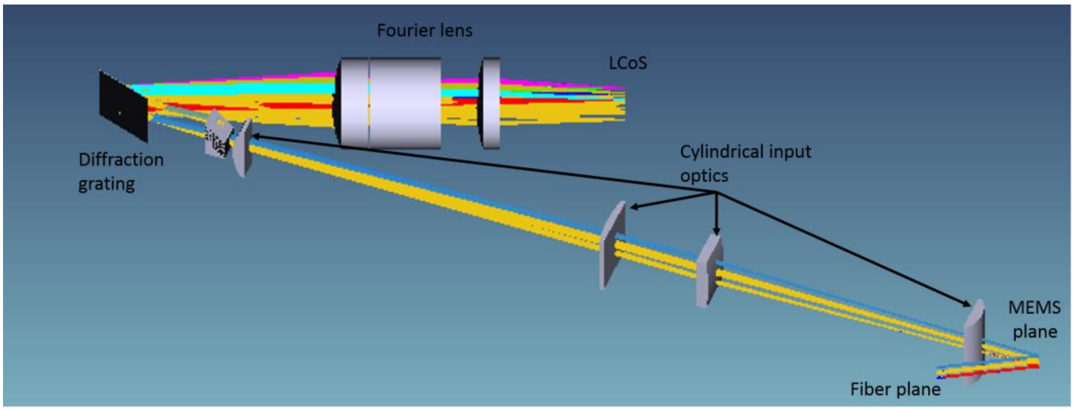

Fig. 2.1.1: Fiber to LCoS propagation.

2.1.1 Fiber to diffraction grating propagation

The target, of this part, is to guide the light beams from the input fiber array to the compatible coordinates (per port) on the diffraction grating and inducing a unique tilt angle per port.

This part is divided into 3 sub parts:

1) Waist projection from the fiber to MEMS: The collimator array is used for waist projection of the Gaussian beams from the fiber array to MEMS (fig 2.1.1.1). It is important to emphasize that light beams on MEMS remain spatially separated according to input port.

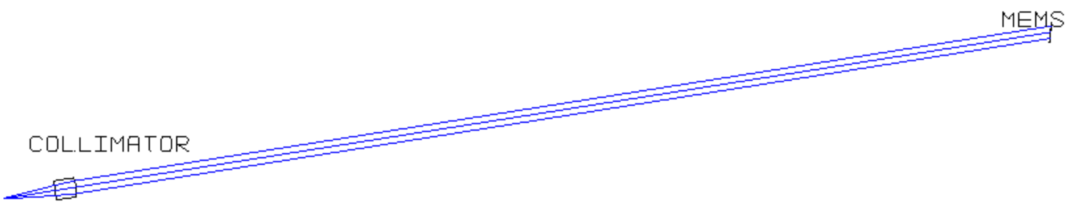

Fig. 2.1.1.1: Fiber to MEMS propagation (top view).

2) Inducing tilt per port: A unique tilt is applied by the MEMS on the light beams according to input port. Therefore, the light beams are angularly separated according to input fiber.

3) Imaging and beam size scaling: The light beams are imaged from the MEMS to the diffraction grating. Cylindrical optics is used for performing it because elliptical spot size (fig 2.1.1.2) is required (detailed explanation in part 3) on the diffraction grating. Therefore, two orthogonal telescopes are being used (fig 2.1.1.3).

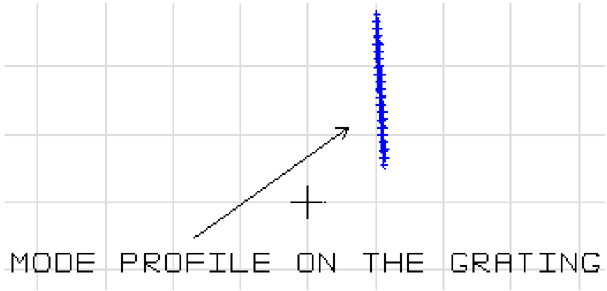

Fig. 2.1.1.2: The elliptical mode profile on the grating

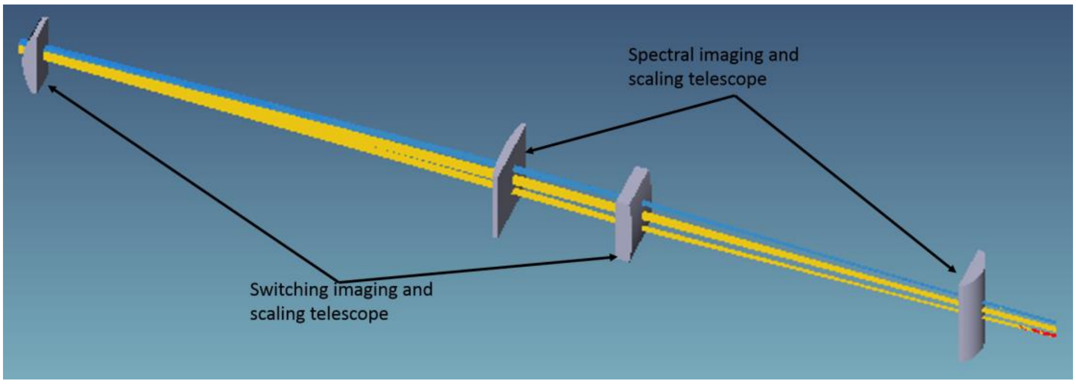

Fig. 2.1.1.3: Orthogonal telescopes.

Note: The light beams are spatially and angularly separated on the diffraction grating because the MEMS plane is imaged onto the grating.

2.1.2 Polarization diversity

The diffraction grating is a polarization sensitive element. Thus, a certain polarization orientation is required for the incident beams on the grating. However, an important requirement for a switch is to be polarization insensitive. Therefore, a polarization diversity assembly is positioned after the cylindrical optics and before the grating.

The polarization diversity assembly is comprised of two elements: PBS (polarization beam splitter) and half wave plate.

1) The PBS separates each beam into its two polarization components (fig 2.1. 2.1).

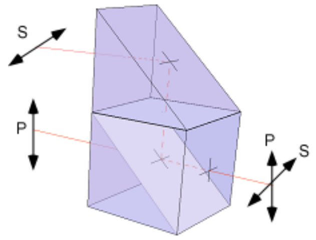

Fig. 2.1.2.1: The PBS separates the beam into its polarization components

2) The half wave plate rotates the polarization orientation of the component which is not compatible with the diffraction grating polarization profile (fig 2. 1.2.2).

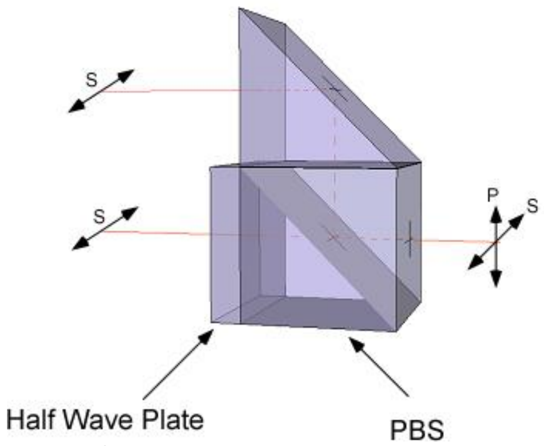

Fig. 2.1.2.2: Beam are co-polarized after passing through the polarization diversity assembly

All the incident light beams on the grating are finally co-polarized. It is important to note the optical path (in the polarization diversity assembly) is not equal for both polarization states. Therefore, the polarization states switch positions, when propagating in the 2nd pass through the polarization diversity assembly in the output part (explained in section 2.3.1), for compensating the different optical path length.

2.1.3 Grating to LCoS propagation

The light beams are being spatially separated on the LCoS SLM according to input port and wavelength channel in this part.

The beams propagate from the diffraction grating (through the Fourier lens) to the LCoS SLM.

This part has to be treated in two orthogonal planes: Switching and dispersion. The propagation in the switching direction will be discussed first.

Switching plane: The incident light beams on the diffraction grating are angularly separated according to input port (section 2.1.1.1). Therefore, the angular separation is transformed into a spatial separation, on the LCoS SLM plane, by the Fourier lens (fig 2.1.3.1).

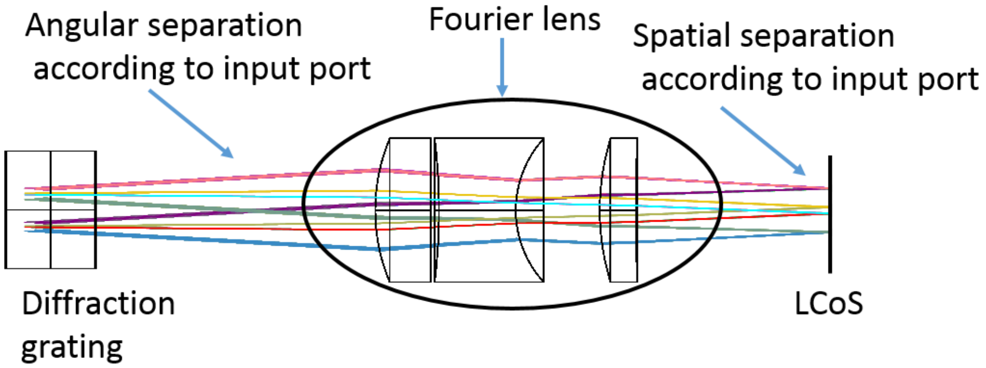

Fig. 2.1.3.1: Diffraction grating to LCoS propagation (Switching plane). Each color represents input port/polarization component.

Dispersion plane: The light beams are angularly separated according to spectral channel after being diffracted from the grating. The Fourier lens transforms the angular dispersion into a spatial dispersion on the LCoS SLM (fig 2.1.3.2).

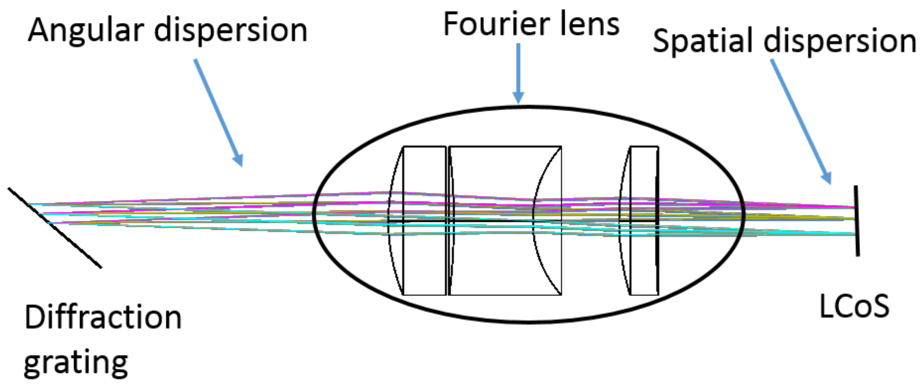

Fig. 2.1.3.2: Diffraction grating to LCoS propagation (Dispersion plane). Each color represents a spectral element.

The layout of beams on the LCoS SLM is shown in fig 2.1.3.3. The light beams are separated according to input port (vertical dimension) and spectral channel (horizontal dimension). Phase function is applied to every grid channel according to the desired switching configuration.

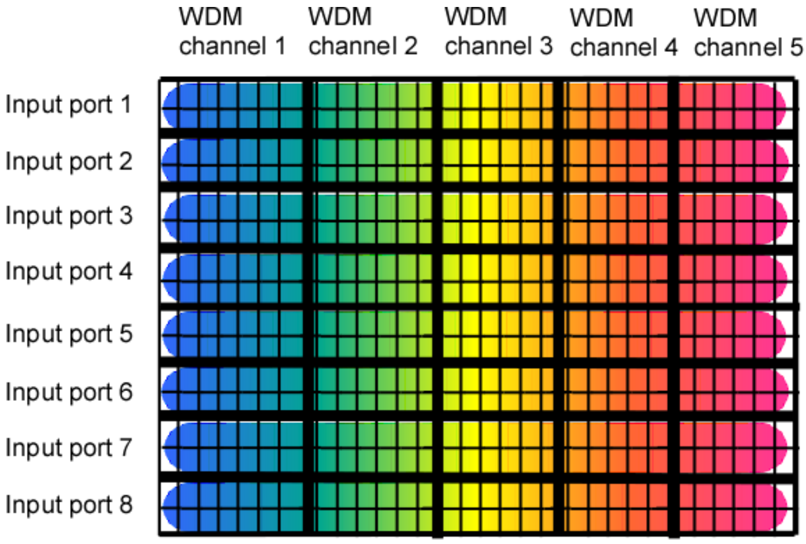

Fig. 2.1.3.3: Beam layout on the LCoS. Separation according to input port and wavelength channel.

It is possible to apply a unique phase function on the LCoS SLM to every spectral channel in every port. This enables multi-channel and multi-port switching.

It is important to emphasize that, although fig 2.1.3.3 conceptually represents the spatial separation according to input port and wavelength channel on the LCoS SLM, there is a slight horizontal shift (fig 2.1.3.4) of spectral components according to input port because the incident angle on the diffraction grating varies per port (detailed explanation in section 3.1.2).

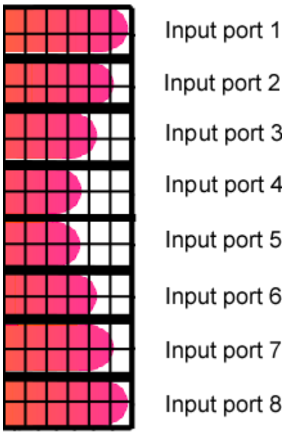

Fig. 2.1.3.3: Horizontal shift of spectral component per port

2.2 Switching part

The target of this part is direct the spectral channels (in every port) to desired output ports.

The light propagates from LCoS SLM to the compatible ports on the grating (There is a unique coordinate for every output port on the grating)

This part will be discusses in both planes as well.

Switching plane: Each spectral element (in every port) is steered independently (except for one restriction) by the LCoS SLM to the compatible output ports on the diffraction grating (fig2.2.1) [6]. The steering angle applied by the LCoS SLM is described in eq 2.2.1

$$\theta_r = \frac{a_{in} + a_{out}}{f} \tag{2.2.1}$$

a_{in}, a_{out} are the coordinates of a specific input and out port respectively on the grating (in the Fourier lens coordinate system) and f is the focal length.

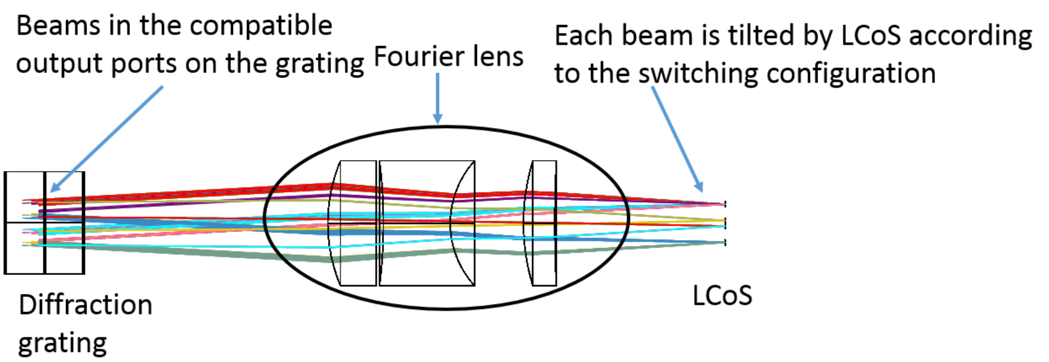

Fig. 2.2.1: Switching part (switching plane).

Dispersion plane: All the spectral elements (in every output port) are imaged onto one spot on the diffraction grating (fig 2.2.2). This is a mirror operation of section 2.1.1.3.

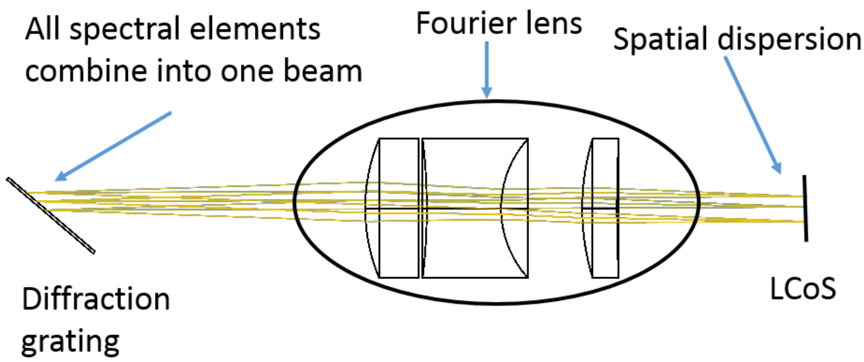

Fig. 2.2.1: Switching part (dispersion plane).

The light beams are now angularly separated according the input port and spatially separated according to output port and polarization (original) orientation. The beam layout on the grating in the output part is shown in fig 2.2.3.

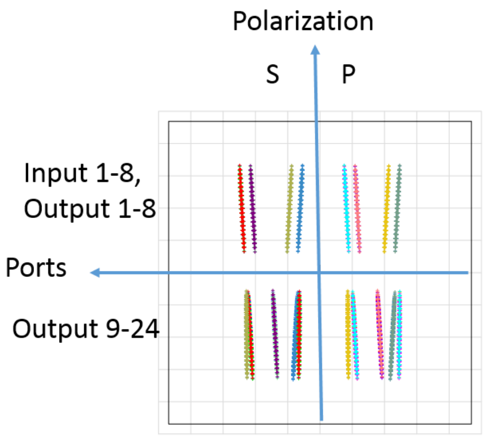

Fig. 2.2.3: Beam layout on the diffraction grating.

2.3 Output part

The light beams propagate from the output ports on the diffraction grating to the compatible output fibers (fig 2.3.1). This part is a mirror operation of section 2.1 (also the same elements are being used).

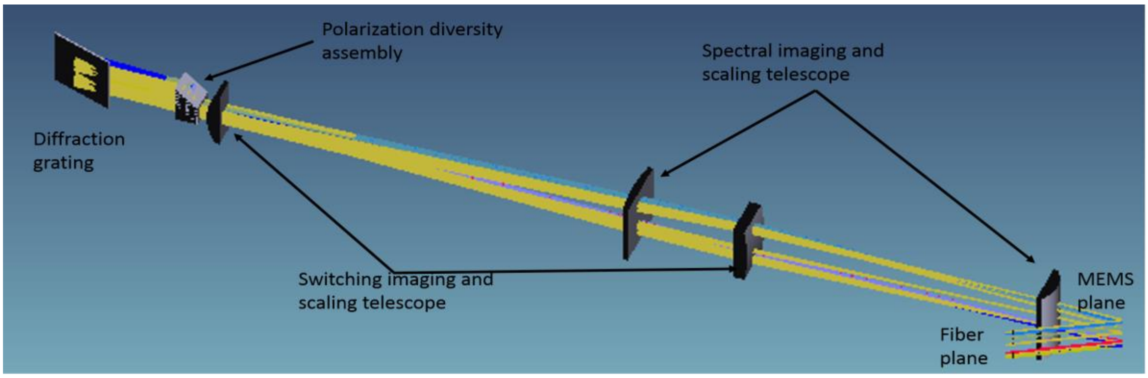

Fig. 2.3.1: Diffraction grating to fiber propagation.

2.3.1 Propagation from the diffraction grating to the MEMS

This part is comprised of 2 sub parts:

1) The polarization elements (for each output port) are combined into one beam by the polarization diversity assembly (fig 2.3.1.1). It is important to emphasize that the polarization states are reversed (the original P comes out as S from the polarization assembly and vice versa) for compensating the optical path difference inflicted after the first pass in the polarization diversity assembly (in the input part).

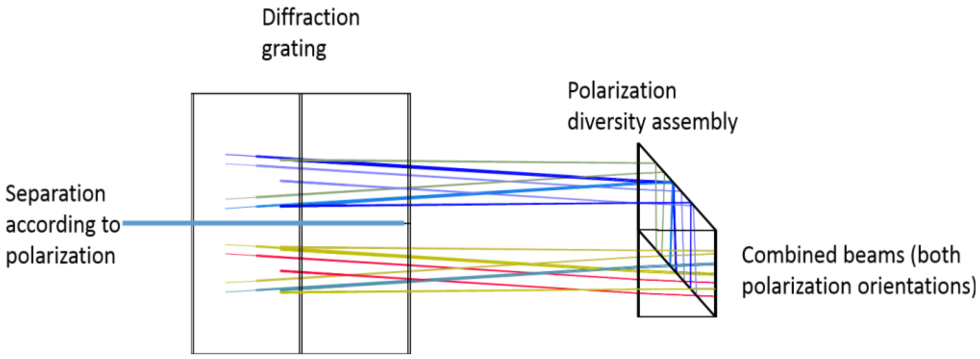

Fig. 2.3.1.1: Polarization states (per output port) are combined into one light beam.

2) The grating plane is imaged to the MEMS plane (fig 2.3.1.2). Therefore, the beams are spatially and angularly separated on the MEMS plane according to output port. The beam profile on the MEMS plane is circular (except a small anamorphic effect) because of the beam rescaling by the cylindrical telescopes in the 2nd pass.

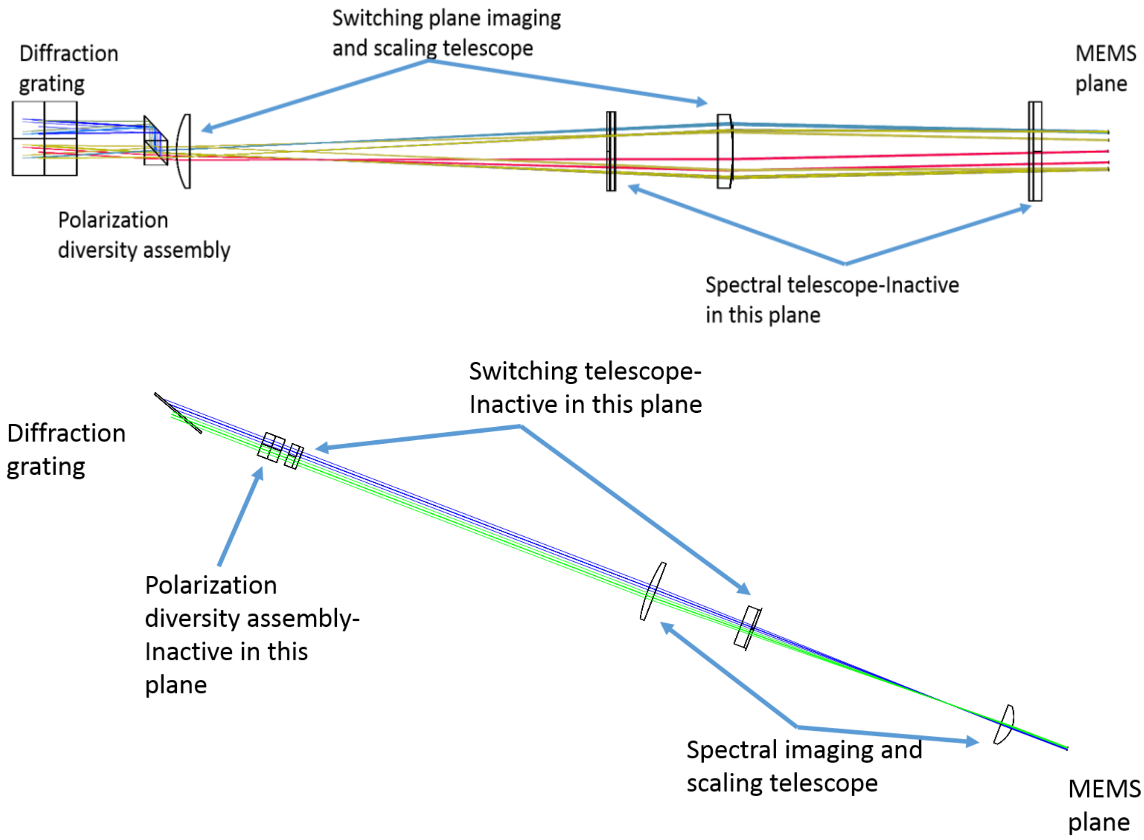

Fig. 2.3.1.2: 2D anamorphic imaging and scaling of the diffraction grating plane to the MEMS plane. Top: side view. Bottom: top view

2.3.2 Propagation from the MEMS to fiber output fiber array.

The incident light beam on the beam are angularly separated according to the input fiber. Therefore, the MEMS mirrors have to realign the beams. This is the reason of the switching restriction, as the mirror cannot simultaneously adjust the mirror angle from two different input ports.

The realigned beams propagate to the collimator array which couples into the fiber array (fig 2.3.2.1).

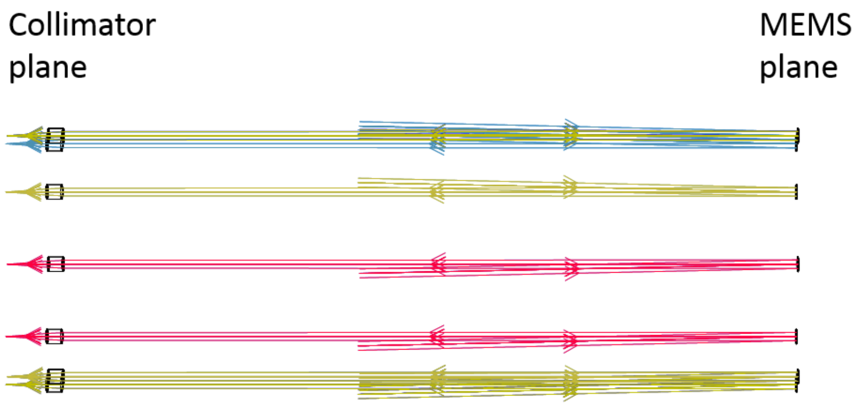

Fig. 2.3.2.1: The MEMS realigns the beam before propagating to the collimator.

3. System analysis

The principle of operation was extensively discussed in the previous section. This part describes the considerations in terms of system engineering.

3.1 Parameters evaluation

The 8x24 is comprised of several elements which some of their properties have to be determined such as:

1) Diffraction grating: Frequency and dimensions.
2) Fourier lens: Focal length value and clear aperture.
3) MEMS array: Tilt angles.
4) Cylindrical optics which determines the anamorphic ratio.
5) Polarization beam splitter: Spatial separation between orthogonal polarizations.

3.1.1 Switching direction parameters

The main parameters, which affect many other decisions regarding system engineering, are the pitch (on the diffraction grating) on the grating and the focal length value (f) of the Fourier lens.

The diffraction grating pitch (p) (fig 3.1.1.1) is the spatial separation between the centers of adjacent ports (in the switching direction) in the grating plane. The minimal value is determined by the 40dB criteria [6] according to $p = 3\omega$ where ω is the mode radius on the diffraction grating.

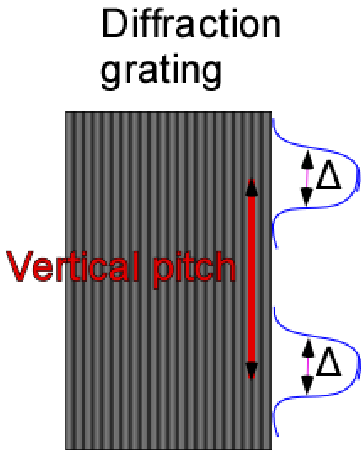

Fig. 3.1.1.1: Vertical pitch between Gaussians (width Δ) from adjacent ports on the diffraction grating.

The pitch and focal length parameters are determined by the steering capabilities and physical dimension of the main dynamic switching element in the system: The LCoS SLM.

The maximal effective steering angle of the LCoS SLM (detailed discussion in section 5) is 2.2° and the dimension of the active area are 15.36mmx8.64mm. Therefore, the following restrictions have to be met:

1) The effective beam aperture on the LCoS SLM has to be smaller than 15.36mm. The pitch (d) and mode diameter (δ) in the LCoS SLM are given in equation 3.1.1.1 [6].

$$d \geq 1.5 \cdot \delta = 1.5 \cdot \frac{\lambda \cdot f}{\pi \cdot \omega} \qquad (3.1.1.1)$$

The effective beam aperture, in the LCoS SLM plane, is $8 \cdot d$.

2) The steering angles(θ) in the switching part have to be less than 2.2°

$$\theta = \frac{a_{1in} - p \cdot (i-1) + a_{1out} - p \cdot (j-1)}{f} \qquad (3.1.1.2)$$

The parameters: i and j are the indices of input and output ports respectively for a desired switching configuration. The height coordinates (in the Fourier lens coordinate system), of the first input and output ports (in the grating plane), are a_{1in} and a_{1out} respectively.

Firstly, we assumed that beam layout on the grating would be a 1D array. However, the restrictions could not be met for this kind of arrangement (as the vertical tilt required is beyond the capabilities of the LCoS SLM). Therefore, we decided that ports will be arranged in a 2D array (fig 3.1.1.2). The required beam steering range (in the switching plane) is smaller for this arrangement.

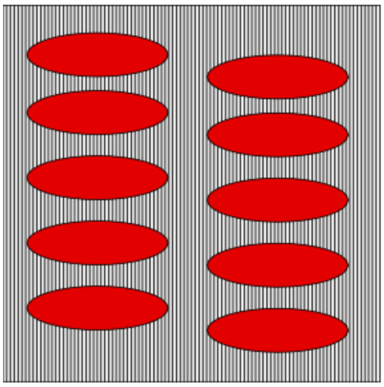

Fig. 3.1.1.2: 2D beam layout on the grating.

The possible p and f values (for the 2D arrangement) were computed by a Matlab program according to the assumptions described above. The results are shown in fig 3.1.1.3. It is important to emphasize that mode size on the LCoS SLM is reciprocal to the p/f ratio (which can be referred to as the system parameter), while the steering angles is linearly proportional to this ratio.

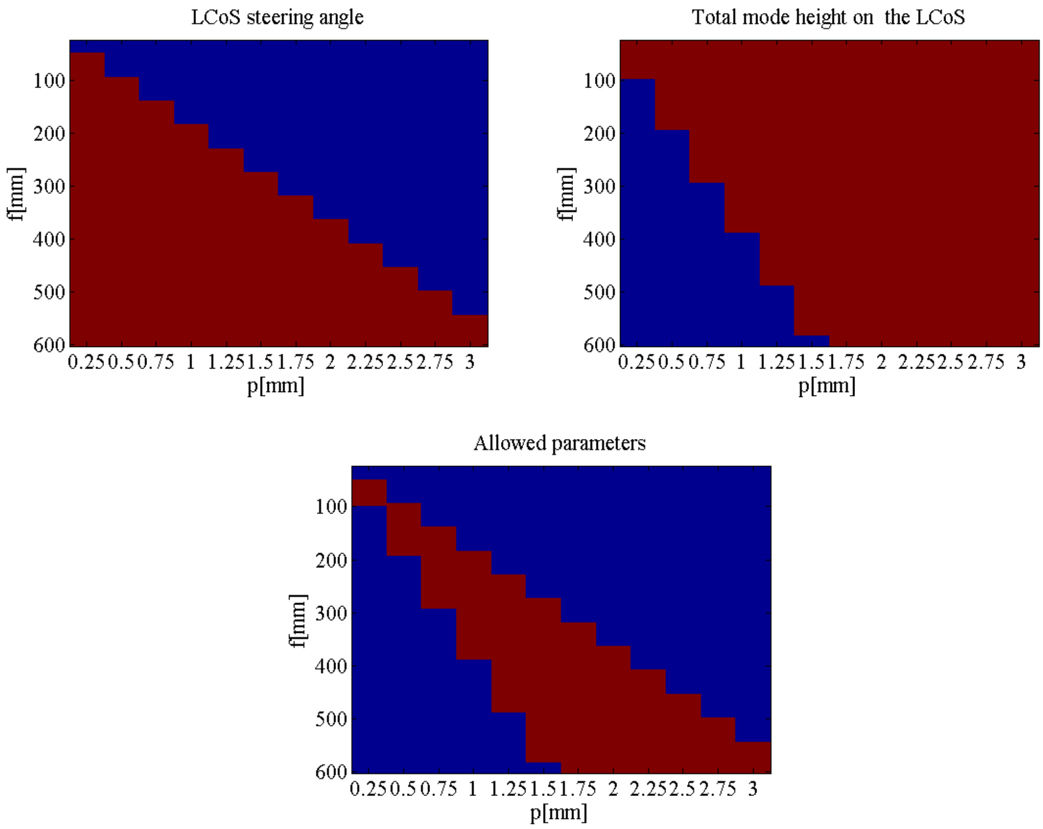

Fig. 3.1.1.3. p and f parameters that satisfy (red color) : Allowed steering angles (top left), allowed total mode height (top right) and all restrictions (bottom).

We have designed a 120mm Fourier lens for the N×N WSXC project (appendix B). Therefore, we wanted to utilize this lens also for the 8×24 WSS.

The allowed pitch value range, assuming a 120m Fourier lens, is 0.3-0.35mm

3.1.2 Dispersion direction parameters

The most important value, which has to be assigned in dispersion plane, is the diffraction grating frequency (f_g). The spectral range (1528.5-1567nm) has to be spatially dispersed in the LCoS SLM plane in the short dimension of this device (8.64mm).

The Fourier lens transforms the angular dispersion range ($\Delta\theta$) (after the diffraction grating as discussed in section 2.1.1.3) into a spatial dispersion (Δx) according to $\Delta x = f \cdot \Delta\theta$. The diffraction angle for a specific wavelength (θ_λ) is described in equation 3.1.2.1[7]. (Assuming the angle of incidence is θ_i)

$$\cos(\varepsilon)\cdot(\sin(\theta_i)+\sin(\theta_\lambda))=\lambda f_g \qquad (3.1.2.1)$$

The diffraction angle depends also on the angle (ε) between the incident light beams to the plane perpendicular to grooves. This leads to horizontal shift of spectral component per port as was described is section 2.1 due to angular separation per input port inflicted by the MEMS micro mirrors. This angle equals zero in conventional WSS designs

The frequency, which meets the requirement (described above), is 1100 lines/mm

The second most important parameter (which is partly derived from the first) is the mode size on the diffraction grating in the dispersion plane. This value (6mm) was computed by available software for WSS design.

3.2 Conclusions in terms of system engineering

The main parameters of the system that were evaluated in the previous section:

1) Diffraction grating pitch-p (0.35mm).
2) Focal length of the Fourier lens –f (120mm).
3) Frequency of the diffraction grating-f_g.
4) Spot size (6mm) on the diffraction grating in the dispersion axis.
5) 2D array spot layout on the diffraction grating.

Firstly, the conclusions regarding the cylindrical optics will be discussed.

3.2.1 Cylindrical optics

The cylindrical optics, which images (and scales) the MEMS plane to grating plane, has to perform the scaling operation which will produce the spot required in 1) and 4).

Therefore, the magnifications of the switching and dispersion telescopes will be $\frac{p}{1.67\Delta} \approx \frac{p}{p_1}$ and $\frac{6}{\beta \cdot \Delta}$ respectively (p_1 and Δ are the MEMS pitch and mode diameter respectively and β is the diffraction grating anamorphic ratio).

3.2.2 Fiber and collimator array layout and pitch

The fiber layout is a 2D array because of requirement 5 as it reduces the beam deflection, in the vertical direction, required by the LCoS SLM.

The waist is to be projected 50mm away from the fiber array which will ensure separation between the collimators array, MEMS and cylindrical optics. The beam size, in the waist position, is 0.6mm. Therefore, the determined fiber pitch value is 1mm which safeties the requirements.

Optical design of the collimator array is discussed in section 4.1.3.

4. Optical design and analysis.

Several optical elements had to be designed for the 8×24 WSS in order to meet the system requirements and for reducing the effect of optical aberrations.

The tool used for designing the system was the Zemax software. The performance testing included geometrical analysis and Physical Optics Propagation (POP) [appendix A].

The following criterions were significant throughout the designing process:

1) Chief Ray deviation at the collimator plane.
2) Chief Ray deviation at fiber plane.
3) Coupling integral calculation at output fiber plane.

4.1 Required optical elements

Optical design was required for the following elements:

1) Fourier lens
2) Cylindrical lenses
3) Collimator array
4) Polarization diversity assembly

4.1.1 Fourier lens

The Fourier lens is an important element in switching systems in general and in the 8×24 WSS in particular.

The Fourier lens must perform well in terms of angle to location conversion (and vice versa) and prevent Gaussian mode distortion for the whole operating wavelength range.

We decided to use the 120mm Fourier lens (fig 4.1.1.1) that was designed for N×N WSXC (appendix B) because some of the system requirements are similar.

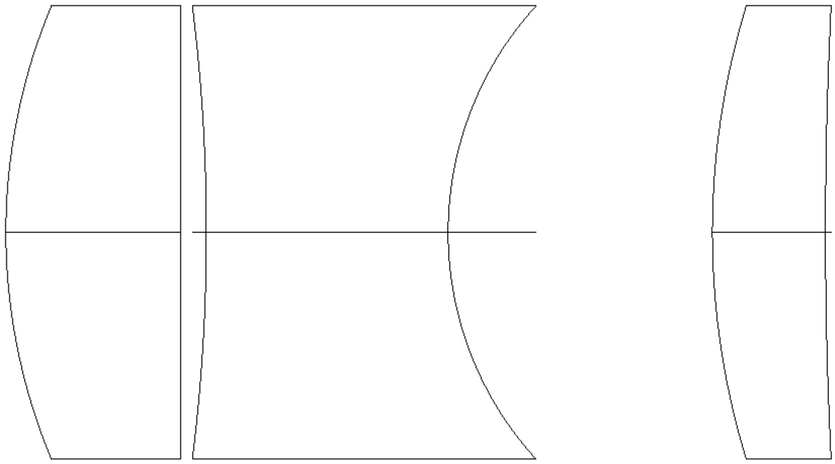

Fig. 4.1.1.1: 120mm Fourier lens.

The lens indeed performed well in the 8×24 WSS as can be seen in the final coupling graph at the end of section 4.

4.1.2 Cylindrical lenses

There are two cylindrical telescopes (operating in orthogonal directions) which create an elliptical Gaussian spot on the diffraction grating (as discussed extensively in section 2.1.1.1). The required magnifications of the switching and dispersion telescopes are ×0.35 and ×5 respectively. Therefore, we decided to use a telescope comprised of 60mm and 175mm lenses in the switching direction and in the orthogonal direction we used a telescope comprised of 150mm and 30mm lenses.

It is important to note that both telescopes are Keplerian and imaging is performed in both planes.

All the cylindrical lenses are Plano-convex and (expect the 175mm) can be found in a Thorlabs catalog.

Only the 175mm lens had to be custom made (by Altechna Company in Lithuania) because there wasn't such lens, in the catalogues, which met our requirements.

4.1.3 2D collimator array

2D collimator array is required in the 8×24 WSS as has been mentioned in the section 3. The layout of the array is shown in fig 4.1.3.1.

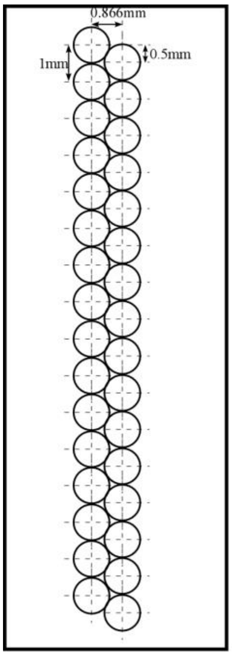

Fig. 4.1.3.1: The 2D collimator array layout.

The collimator was designed in Zemax and its properties are as follows:

1) The focal length value is 3.265mm (for getting 0.6mm mode diameter Gaussian in the MEMS plane).
2) The conic constant is -0.56.
3) The clear aperture is greater than 90% for reducing the truncation effect.

The specifications of the array are as follows:

1) Two columns
2) Sixteen collimators per column.
3) The vertical pitch is 1mm
4) The vertical offset, between the columns, is 0.5mm.
5) The horizontal offset, between the columns, is 0.866mm.

4.1.4 Polarization diversity assembly

Another element which was custom made, for the 8×24 WSS project, is the polarization diversity assembly.

This assembly is comprised of polarization beam splitter and a half wave plate (as described in section 2.1.1.2)

Altechna Company manufactured the assembly according to our requirements:
1) 10mm separation between the polarizations
2) 10mm×20mm are the dimension of the entrance face.
3) The thickness of the cube is 10mm.

4) The output polarization is ‘S’.

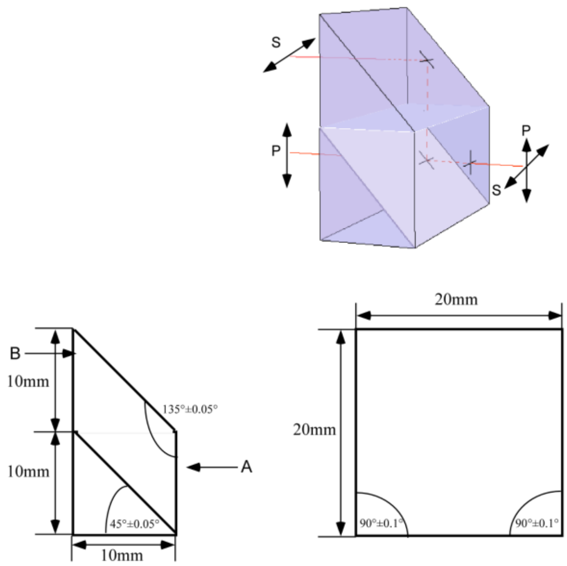

Fig. 4.1.3.1: The 2D collimator array layout.

4.2 The LCoS as a coupling improvement tool

The LCoS SLM proved to be an effective tool in aberration correction by applying a phase function which was the inverse Zernike polynomial of the tested system [8].

We examined the possibility of applying curved phase function by the LCoS SLM for the purpose of aberrations (and assembly errors) compensation which leads to coupling improvement.

The LCoS SLM was modeled in Zemax as curved mirror (which applies curvature and tilt angle).

The 8×24 WSS was tested in Zemax. Several representative switching configurations and wavelengths were examined in terms of Gaussian power coupling (It is important to note the Zemax treats the coupling inflicted by optical aberrations).

The performance of 8×24 WSS is slightly better when curved phase function is applied by the LCoS SLM (fig 4.2.1)

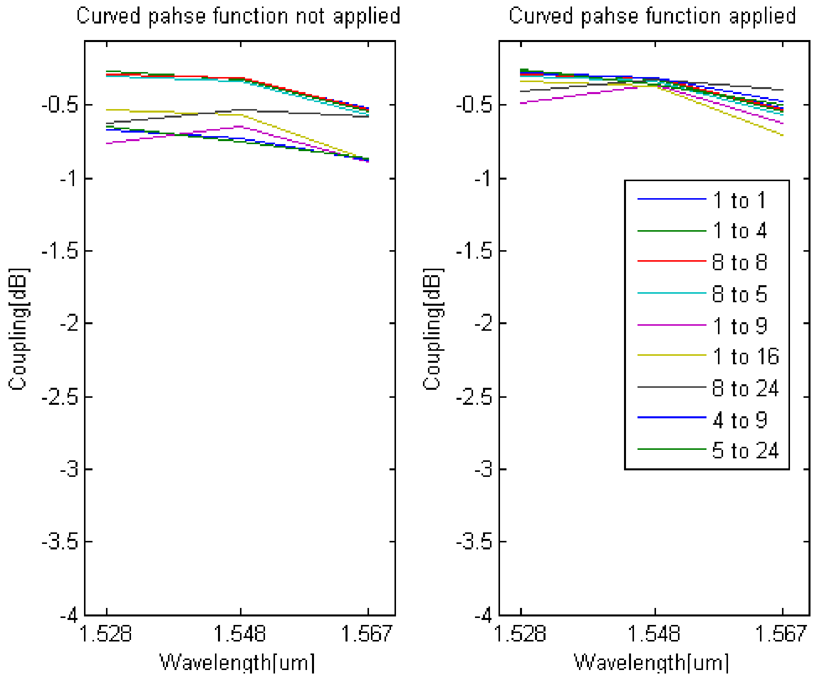

Fig. 4.2.1: Coupling performance. Left: Curved phase function not applied. Right: Curved phase function applied. Legend: Switching configurations

The performance in terms of PDL (Polarization Dependent Loss) is better as well when phase function is applied by the LCoS SLM.

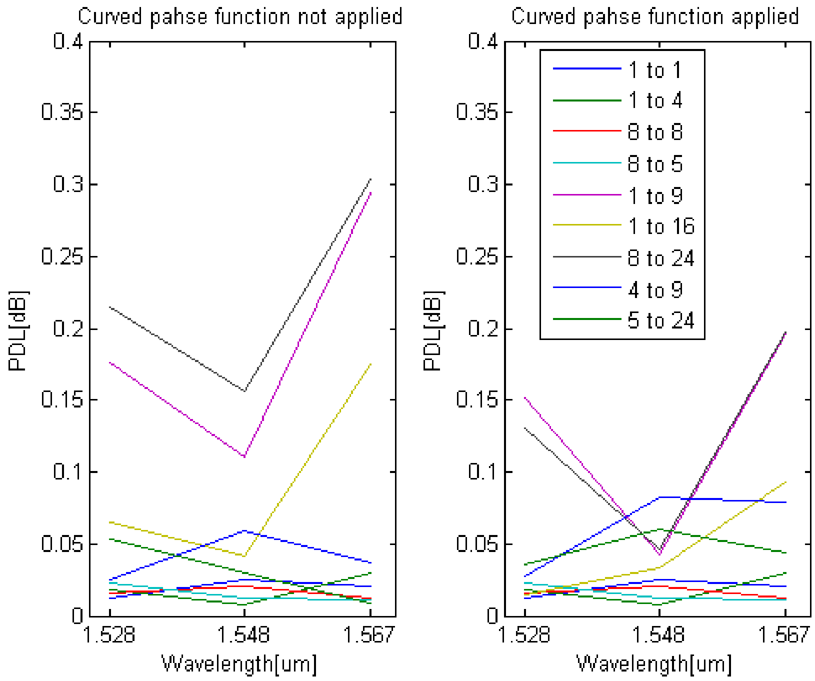

Fig. 4.2.2: Coupling performance. Left: Curved phase function not applied. Right: Curved phase function applied

The Zemax simulation showed that performance is indeed improved when curved phase function is applied by the LCoS SLM. Therefore, it can be utilized also as an aberration compensation element, not only as a dynamic steering device.

5. LCoS experiment

5.1 Introduction

The characterization experiment of the Holoeye LCoS SLM, the dynamic steering element, will be introduced in this part.
The goal of this experiment is to investigate the LCoS SLM in terms of maximum steering angle and crosstalk levels.
The maximum steering angle, which corresponds to the minimal number of pixels per period, is of tremendous importance to the switch since it effects the possible values of the systems' parameters: *f* and *p*.
The description of the setup (fig 5.1): Gaussian beam, from the fixed collimator, is focused (by Fourier lens) on the LCoS which applies on it steering phase function that routes the light towards the mobile collimator. The measurement was repeated for several Fourier lens focal lengths.

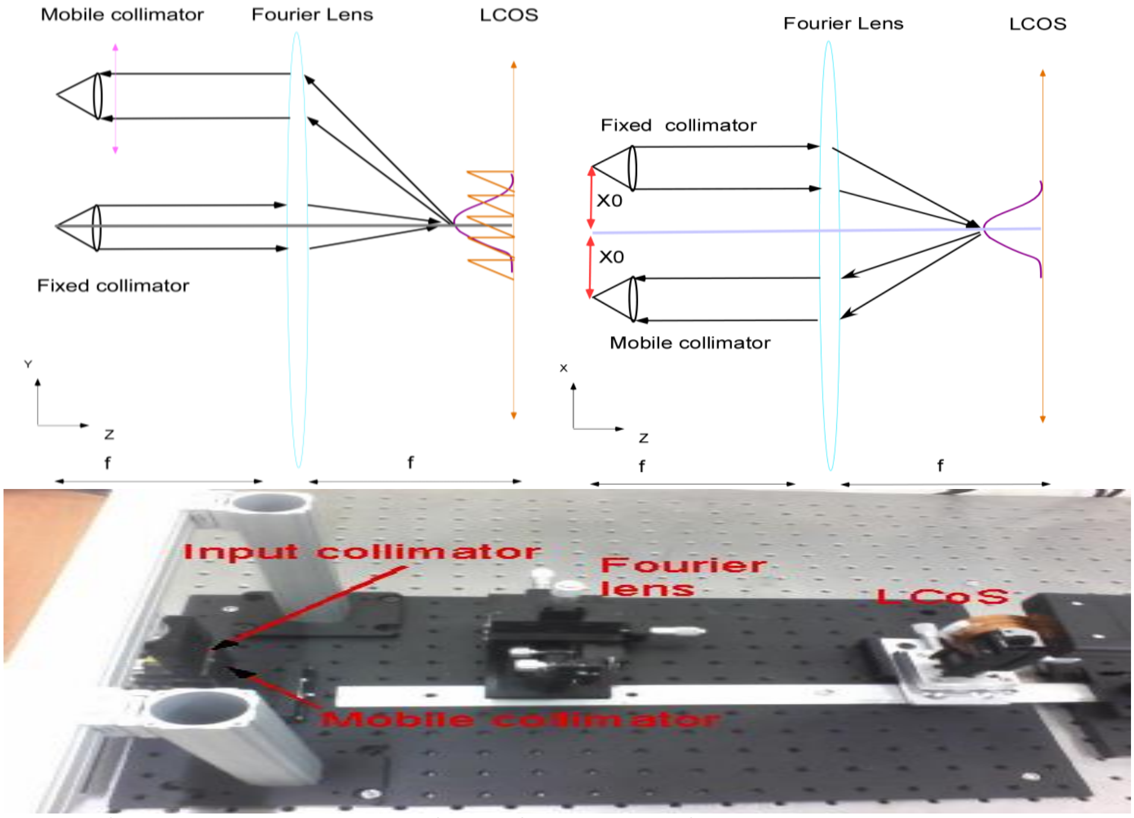

Fig 5.1. Left (Top view): The propagated light from the fixed collimator is focused by the Fourier lens on the LCoS which applies a tilt on the beam required for routing towards the mobile collimator. Right (side view): The collimators are located in equidistance from the optical axis. Therefore tilt is not applied in this direction. Bottom: Picture of the setup.

5.2 Experimental Results

5.2.1 Coupling

The coupling efficiency dependence on the steering angle of the LCoS SLM is very important for the parameter evaluation of the switch.

The sawtooth (example in Fig. 5.2.1.1)) function is generated on the SLM for the purpose of steering. The deflection applied (θ) on the beam depends on the number of pixels per period (Λ) according to $\Lambda = \frac{\lambda}{\theta \cdot pixel\_size}$ [6]. The minimum criterion of Λ was set to be 5 (corresponds to max steering angle of 2.2° described in section 3.1.1).

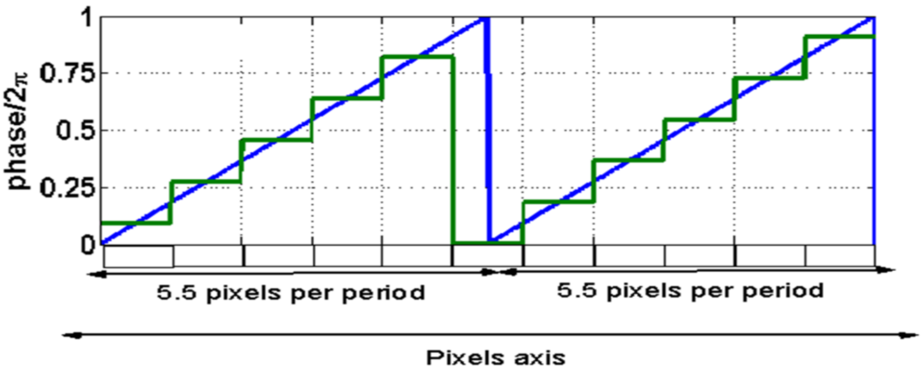

Fig 5.2.1.1: An example of saw tooth function with Λ=5.5. Green: panelized function. Blue: The theoretical function

The steering experiment was repeated for Fourier lenses of focal lengths of 75 and 150 mm and the angular range of the generated phases was -3°:0.023°:3°. The mobile collimator was located on a translation stage and the movement was controlled by computer. The results for the f=75mm lens are shown in fig 5.2.1.2

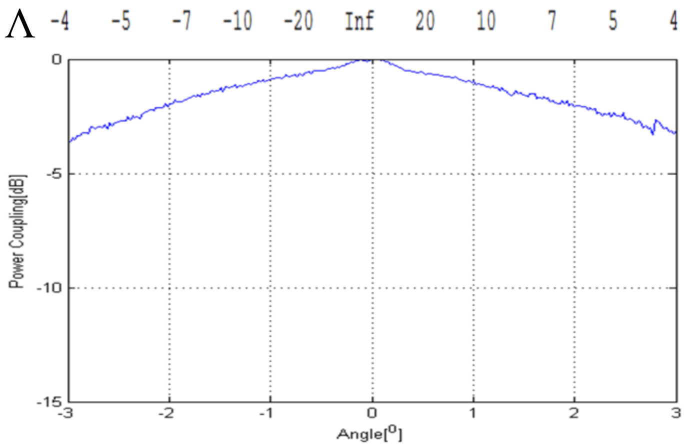

Fig 5.2.1.2. *f*=75mm results: Power coupling vs. SLM deflection (bottom *x* axis) and Λ (upper y axis).

The coupling results for the setup with the *f*=150mm were much worse than for the *f*=75mm. Theoretically, the coupling efficiency depends only on the tilt phase function. Therefore, it was suspected that there is a rotational misalignment between the LCoS panel and the collimator translation axis. This assumption was experimentally verified in the following manner: Tilt function was applied also in orthogonal plane which resulted in coupling improvement of up to 5dB as depicted in figure 5.2.1.3

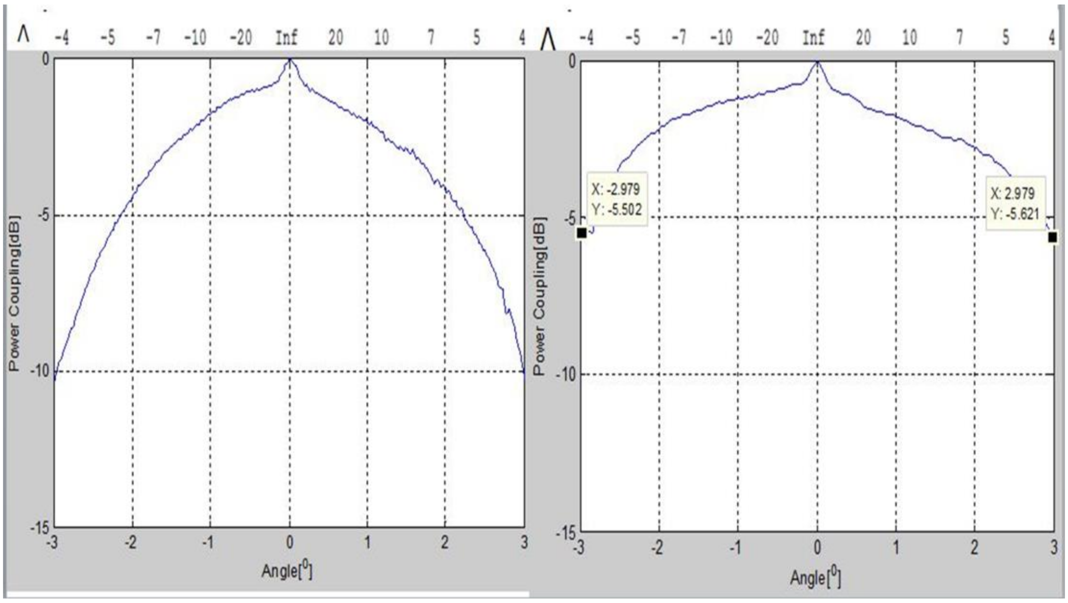

Fig 5.2.1.3. Left: Tilt was not applied in the orthogonal direction. Right: Tilt was applied in the orthogonal direction

The effect of angular misalignment is more prominent for longer focal lengths because the value of the spatial translation is greater according to $y = f \cdot \theta$, where θ is the LCoS roll, which leads to quadratic exponential (~exp[-(y/w)^2]) decay of the power coupling. Therefore, tilt has to be applied in the orthogonal direction as well (especially for high focal lengths).

5.2.2 Crosstalk

The crosstalk issue was investigated as well in this experiment. For each SLM deflection the power was measured in locations (angles) other than the target. The measuring locations (corresponding to the compatible angles) resolution was identical to phase generation resolution for both focal lengths. It is important to emphasize that crosstalk is reduced by the switch design according to feature of the system described in section 5.4.
All the results for both focal lengths are shown below:

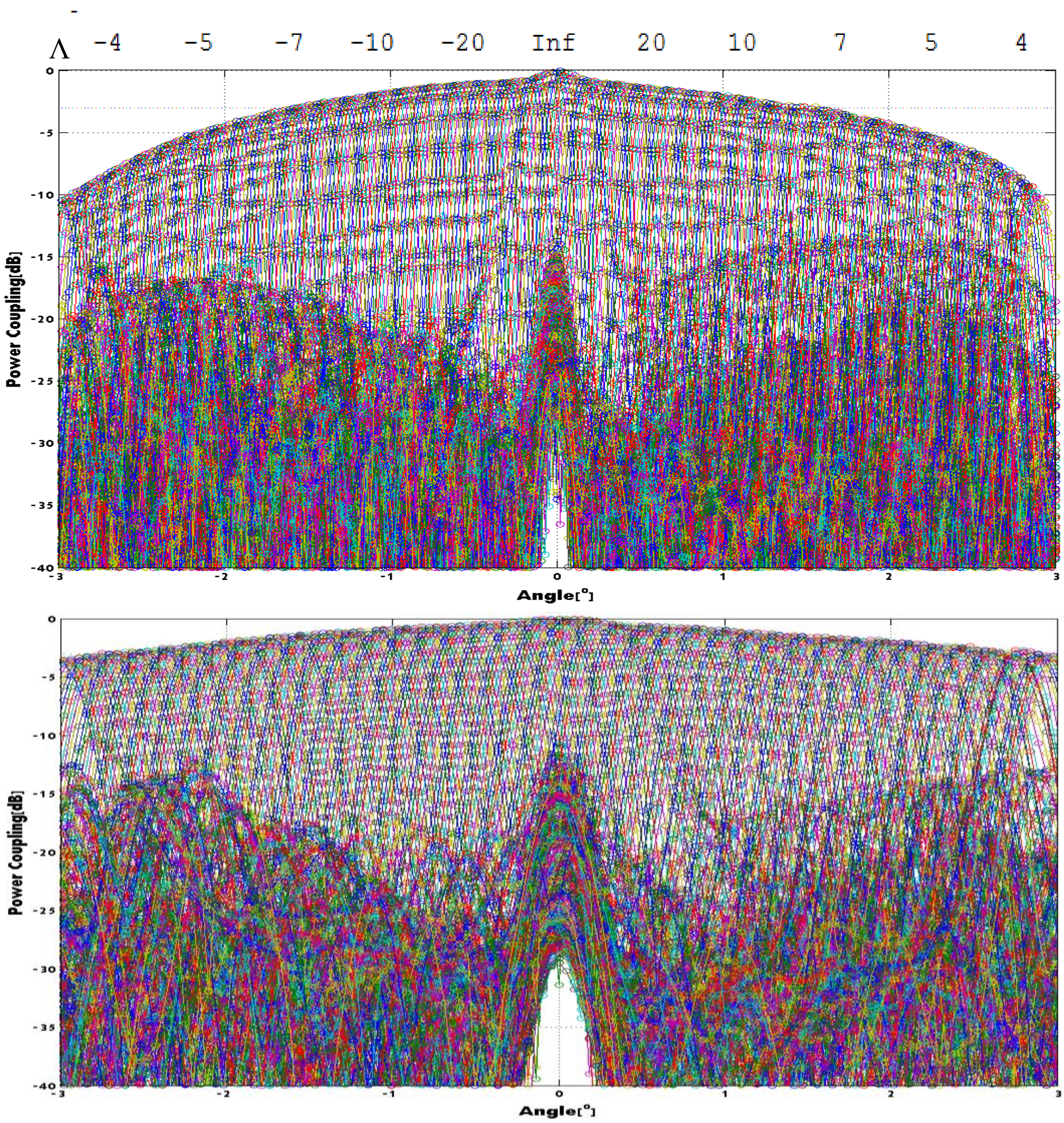

Fig 5.2.2.1. Each curve represents the power measurements at all locations (angles) for a single SLM deflection. Top: f=150mm (no roll elimination was applied here, hence the rapid roll off). Bottom: f=75mm.

The crosstalk will be discussed in following sub categories: Low (<0.2°) and high deflection angles, integer and non-integer periods.

5.2.2.1 Low deflection angles

The value of Λ, for low steering angles, is very high. Therefore the sawtooth phase function is well sampled. This yields to the elimination of the higher diffraction orders as depicted in fig 5.2.2.1.1

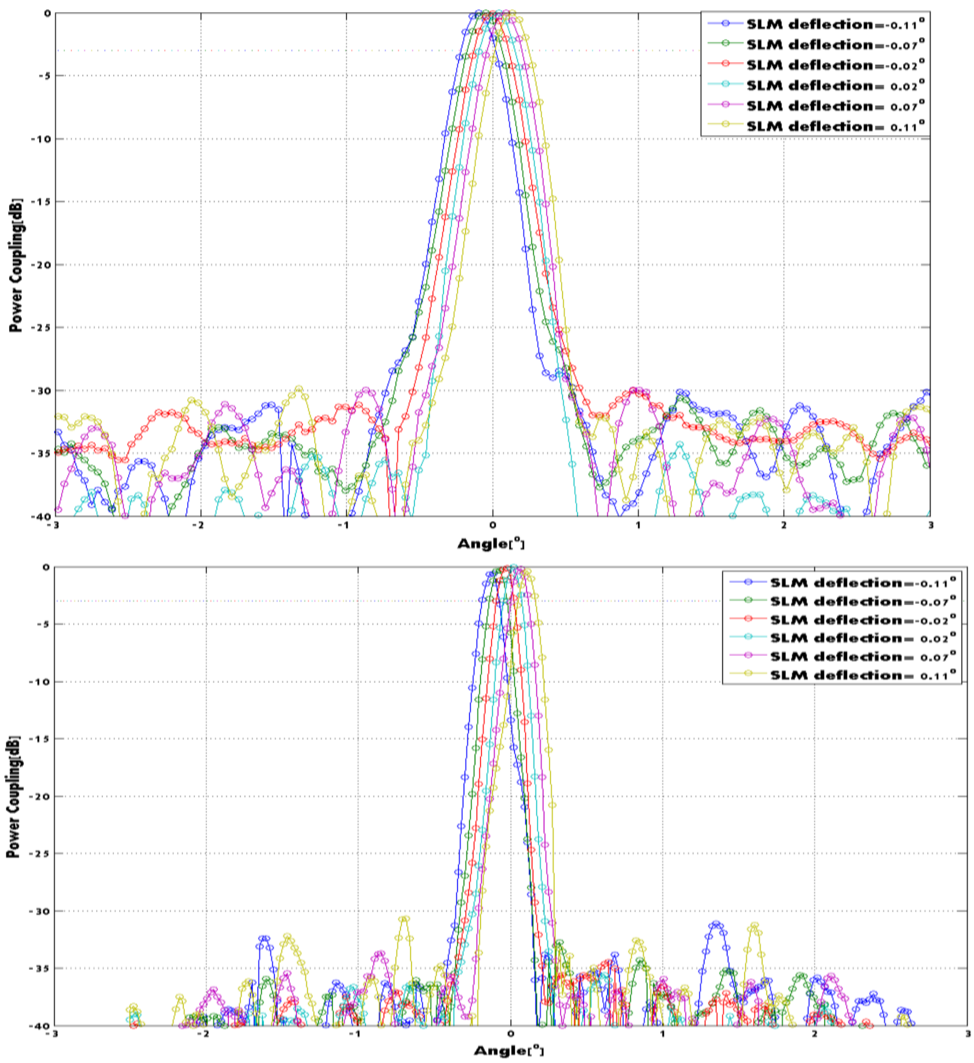

Fig 5.2.2.1.1: The diffraction orders are eliminated for low deflection angles. Top: f=75mm.Bottom: f=150mm

The power peaks are measured at random locations which don't correspond to the diffraction orders. Therefore, the diffraction effect is negligible.

5.2.2.2 Diffraction affected angles

The blazed grating period is sampled by fewer pixels for higher deflection angles. Therefore, the diffraction effects become the prominent crosstalk source for this case as depicted in the example below:

Fig 5.2.2.2.1: An example of diffraction affected SLM deflection. The power peaks correspond to integer multiples of the target angle.

The crosstalk gets worse for larger steering angles (fig 5.2.2.2.2)
The crosstalk is greater for higher deflection angles especially in the ±2 diffraction orders

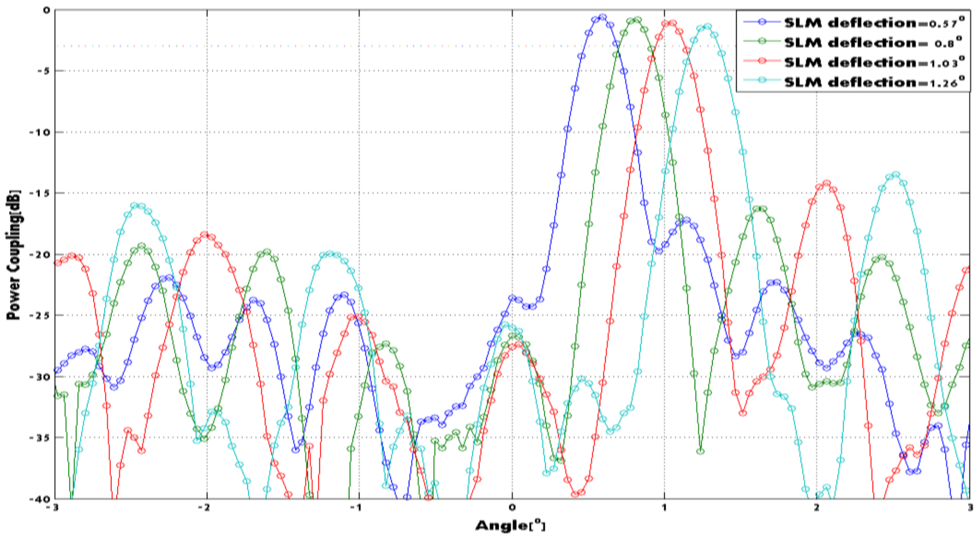

Fig 5.2.2.2.2: An example of crosstalk levels variation for greater deflection (f=75mm)

5.2.2.3 Integer and non-integer periods

Semi integer diffraction orders might be prominent for tilts corresponding to non-integer values. The crosstalk might be reduced as energy will be transferred from the integer (the main crosstalk source) to the non-integer orders.

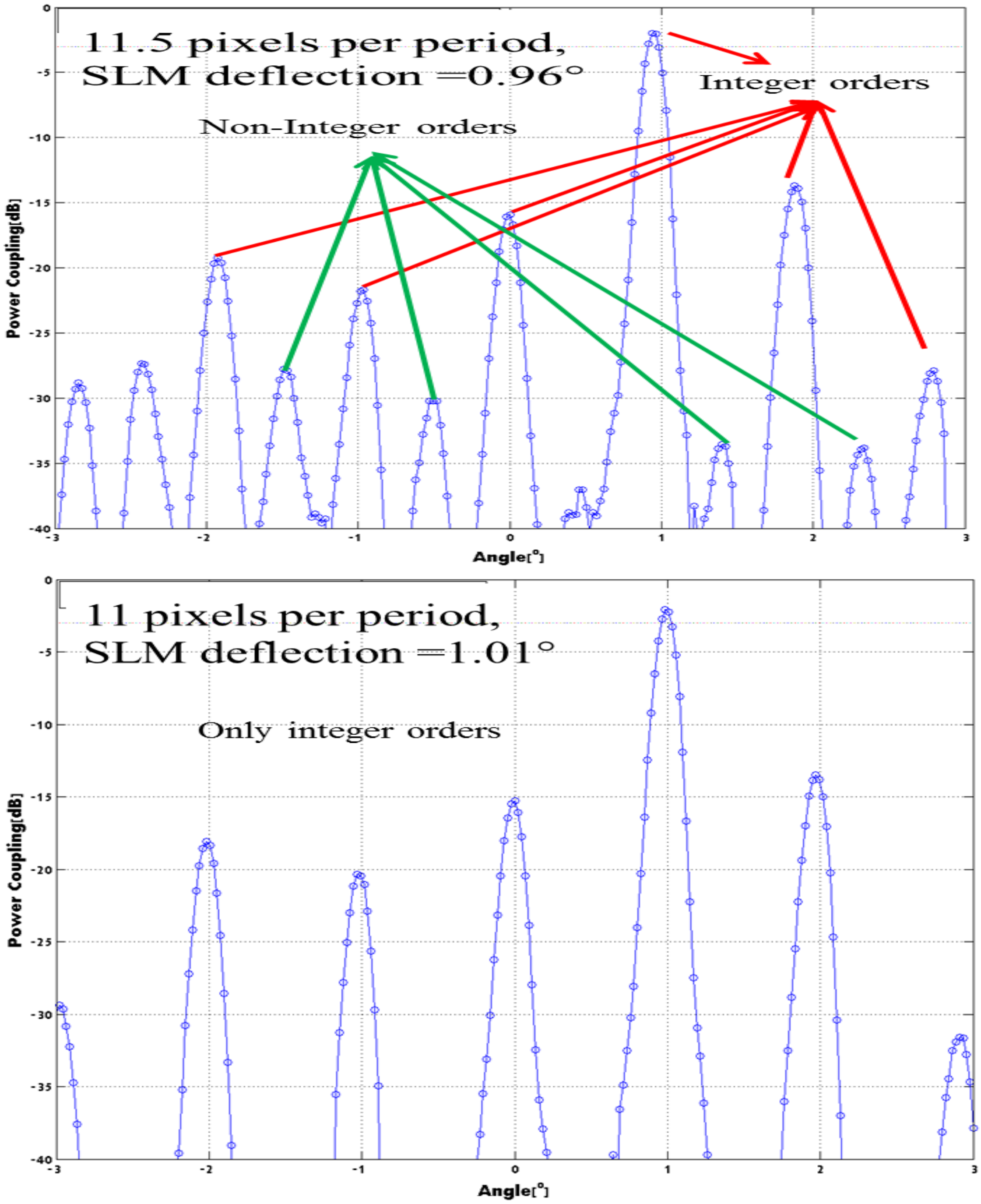

Fig 5.2.2.3.1: Non-integer (top) vs. Integer (bottom) periods

The semi diffraction orders appeared indeed for small period but the crosstalk levels didn't vary significantly.

This phenomenon seems to be negligible for larger periods (>20) as depicted in the figure below. Note that the beam size is about 100 pixels.

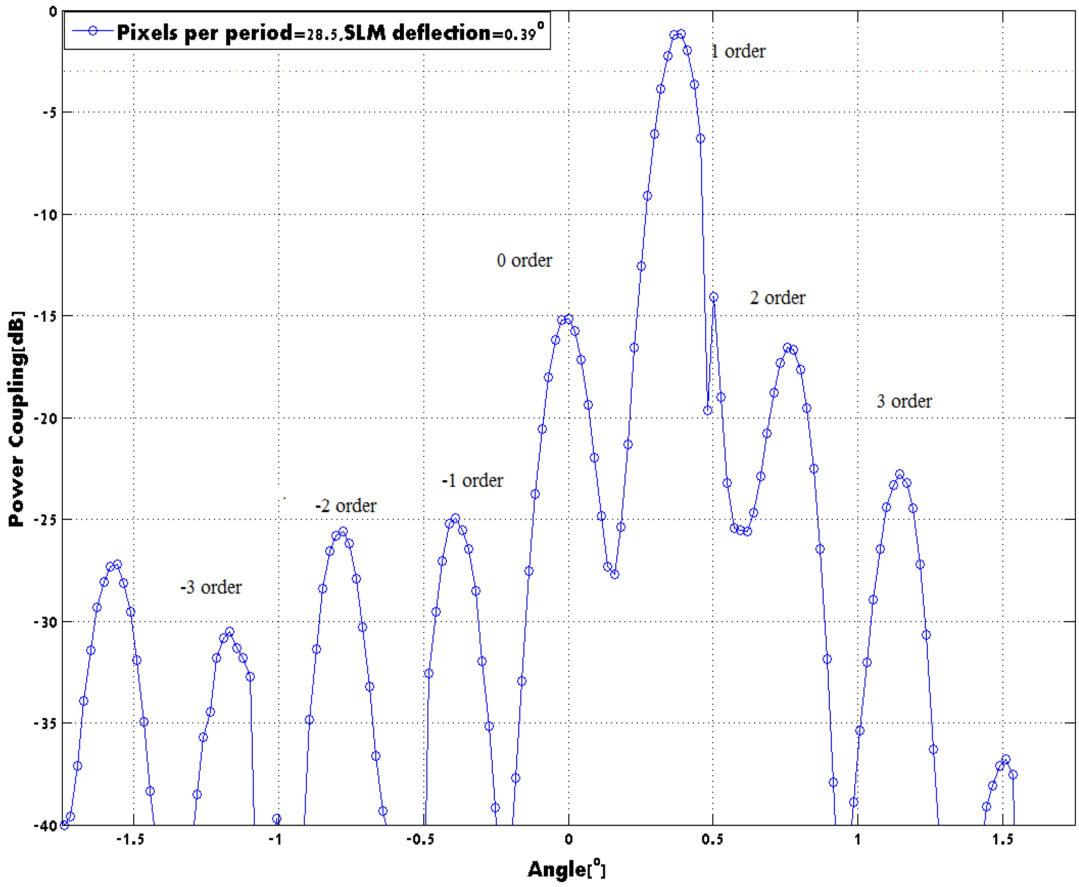

Fig 5.2.2.3.2. The semi periods are not prominent for this non-integer period of 28.5 (SLM deflection =0.39°)

It seems that semi integer do not contribute much to the crosstalk reduction

5.2.3 Pixel perturbation experiment

The true nature of the phase in the transient region from 2π to 0 (between 2 adjacent periods) is not clear and is influenced by electrical fringing fields and the LC physical properties. The effect of perturbation of phase values of pixels in this region was examined to see if performance (IL, PI) can be improved.

The values of the first, second, second last, last pixels, of each period, were perturbed (figure below).

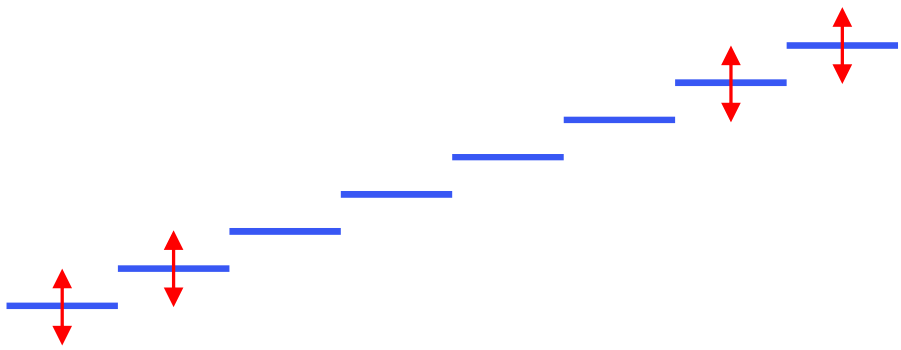

Fig 5.2.3.1. An example of pixel perturbation experiment: The phase values of first, second, second last and last pixels are varied

The phase value of each pixel (of the described above) was perturbed independently by the following 7 values: -0.15π, -0.10π, -0.05π, 0π, 0.05π, 0.1π, 0.15π. This was done independently to each of the four pixels (7^4 trials).
Three different deflections, corresponding to periods of 14(0.8°), 10(1.1°) and 8(1.4°) pixels were generated.
The experimental setup: The LCoS steering setup (f=150mm).
The results are presented in the following manner:
For each deflection a table and a graph of the unperturbed state are presented
Table description:

1) The values of the IL (Insertion Loss) and PI (Port Isolation-the difference between coupling and crosstalk) are presented for the unperturbed state (no attempt of correction) in the second line.

2) The values of the IL, PI and the perturbation configuration, for the best case of the optimization assuming that -2, 2 orders are ignored(are outside our field of view), are presented in the third line. This corresponds to the case when tilting to large angles or edge ports (higher orders are outside of view).

3) The values of the IL, PI and the perturbation configuration, for the best case of the optimization assuming that all orders are taken into account, are presented in the third line. This corresponds to the case when tilting to small angles or inner ports.

<u>8 pixels (1.4° tilt, π/4 phase step height)</u>

The performance of for period of 8 pixels is shown it the table and figure below:

Perturbation configuration	**2** **IL[dB]** **PI[dB]**	**1** **Target IL[dB]**	**0** **IL[dB]** **PI[dB]**	**-1** **IL[dB]** **PI[dB]**	**-2** **IL[dB]** **PI[dB]**	**Order**
No perturbation applied	-12.36 10.28	-2.08	-16.14 14.06	-17.65 15.57	-18.22 16.14	Non perturbed
0.15π,0.15π, 0.1π, -0.1π	**Ignored**	-1.91	-30.36 28.45	-26.16 24.25	**Ignored**	-1,0,1 optimization
0.15π, 0.15 π, -0.1π, 0.15π	-18.95 17.21	-1.74	-19.58 17.84	-31.03 29.29	-21.57 19.83	-2,-1,0,1,2 optimization

The PI improved significantly for both optimizations

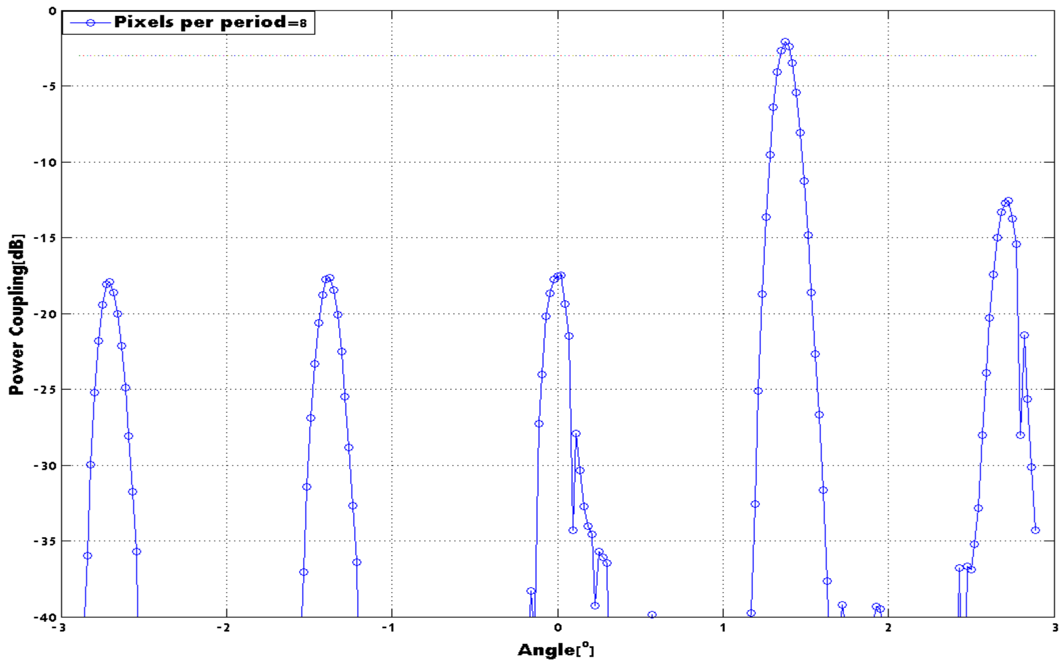

Fig 5.2.3.2: The results of the unperturbed state for the 8 pixel per period SLM deflection

10 pixels (1.1° tilt, π/5 phase step height)

Perturbation configuration	**2 IL[dB] PI[dB]**	**1 Target IL[dB]**	**0 IL[dB] PI[dB]**	**-1 IL[dB] PI[dB]**	**-2 IL[dB] PI[dB]**	**Order**
No perturbation applied	-13.15 11.34	-1.81	-15.13 13.32	-19.94 18.13	-17.12 15.31	Non perturbed
0π, -0.15 π, 0.15 π, 0.15π	**Ignored**	-1.55	-21.43 19.88	-24.71 23.16	**Ignored**	-1,0,1 optimization
0.1π, -0.1 π, 0.15π, 0.15π	-18.19 16.69	-1.50	-19.66 17.16	-30.16 28.66	-18.36 16.86	-2,-1,0,1,2 optimization

The improvement of the PI for this case is not as well as the previous one.

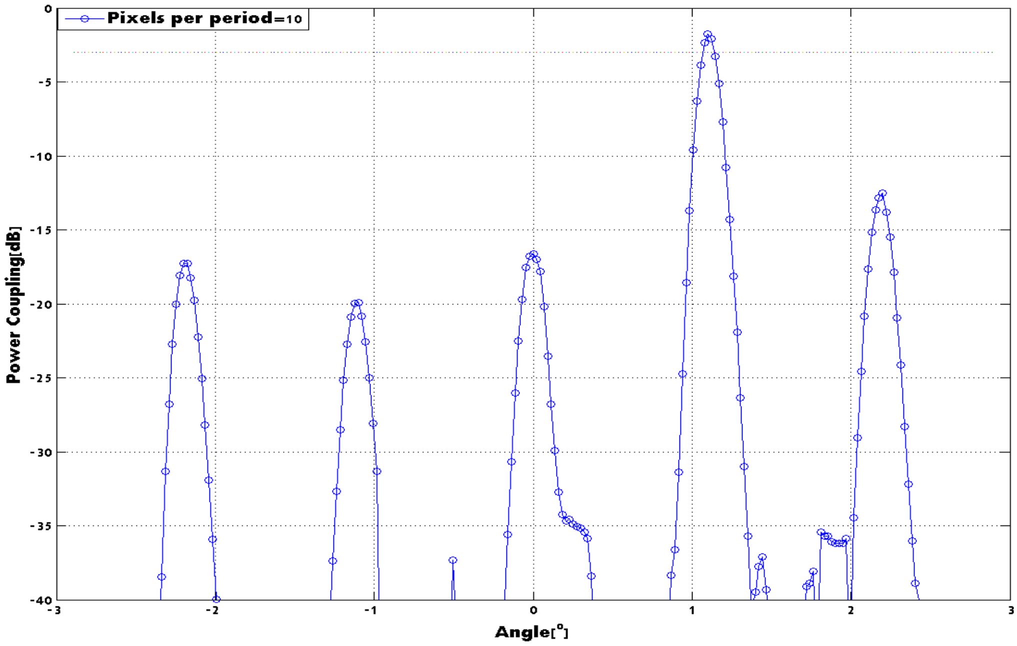

Fig 5.2.3.3: The results of the unperturbed state for the case of 10 pixels per period perturbation

<u>14 pixels (0.8° tilt, π/7 phase step height)</u>

Perturbation configuration	**2 IL[dB] PI[dB]**	**1 Target IL[dB]**	**0 IL[dB] PI[dB]**	**-1 IL[dB] PI[dB]**	**-2 IL[dB] PI[dB]**	**Order**
No perturbation applied	-13.15 11.34	-1.81	-15.13 13.32	-19.94 18.13	-17.12 15.31	Non perturbed
0.15π, 0.05 π, -0.15 π, -0.15π	**Ignored**	-1.55	-21.43 19.88	-24.71 23.16	**Ignored**	-1,0,1 optimization
-0.15π, 0.05 π, -0.15π, -0.15π	-18.19 16.69	-1.50	-19.66 17.16	-30.16 28.66	-18.36 16.86	-2,-1,0,1,2 optimization

The performance improvement for this case was the least.

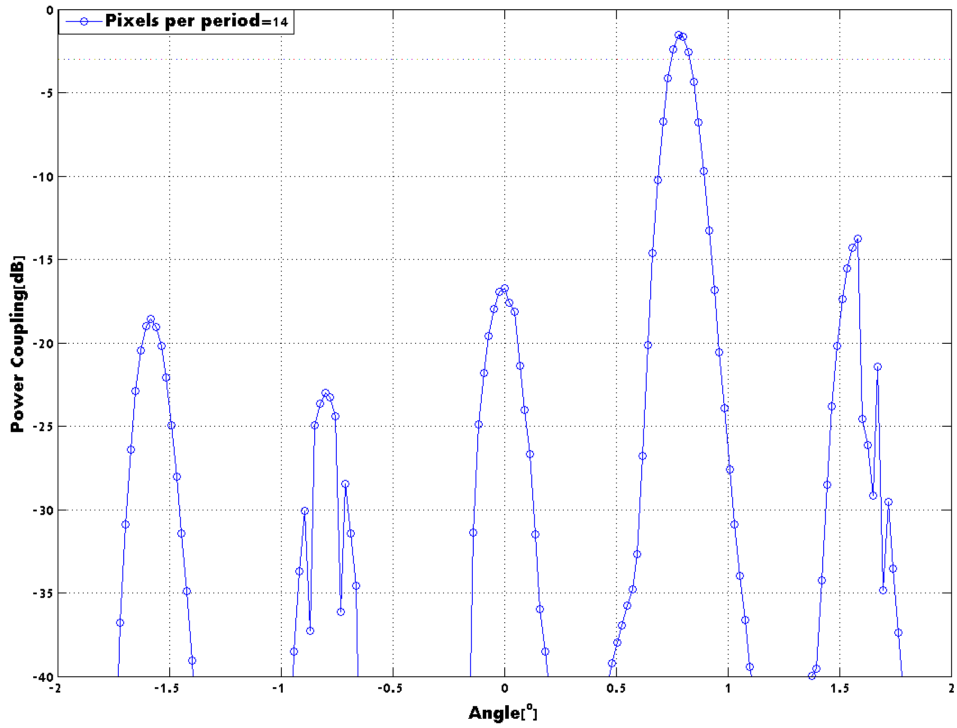

Fig 5.2.3.4: The unperturbed state for the case of 14 pixels per period deflection

<u>Conclusions</u>

1) The performance of the optimization increase for higher SLM deflections

2) The following future experiments might contribute for better understanding of the effectiveness of the this optimization :

    1) Repeating the experiment for more tilts.

    2) Repeating the experiment for more perturbation values (not only multiple integers of 0.05π).This will enable us investigating the dependence of the required correction values on the phase step heights.

5.2.4 Diagonal tilt

Another method for crosstalk reduction was investigated. The symmetry (depicted in fig 5.1.1 side view) in the orthogonal direction was cancelled. Thus, the input and output collimators were no longer equidistant from the optical axis (in the orthogonal direction). Therefore, a tilt has to be applied also in the orthogonal direction.

The axis of the diffraction orders, for this case, does not coincide with the scanning axis of the mobile collimator (fig 5.2.4.1).

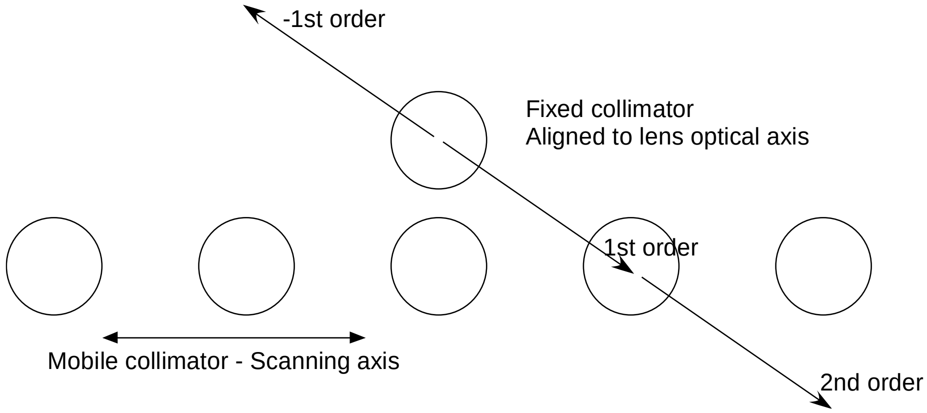

Fig 5.2.4.1: The axis of diffraction orders does not coincide with the scanning axis in the new collimators arrangement.

The input collimator was aligned with the optical axis and 17 SLM deflections were generated. The results are presented in fig 5.2.4.2

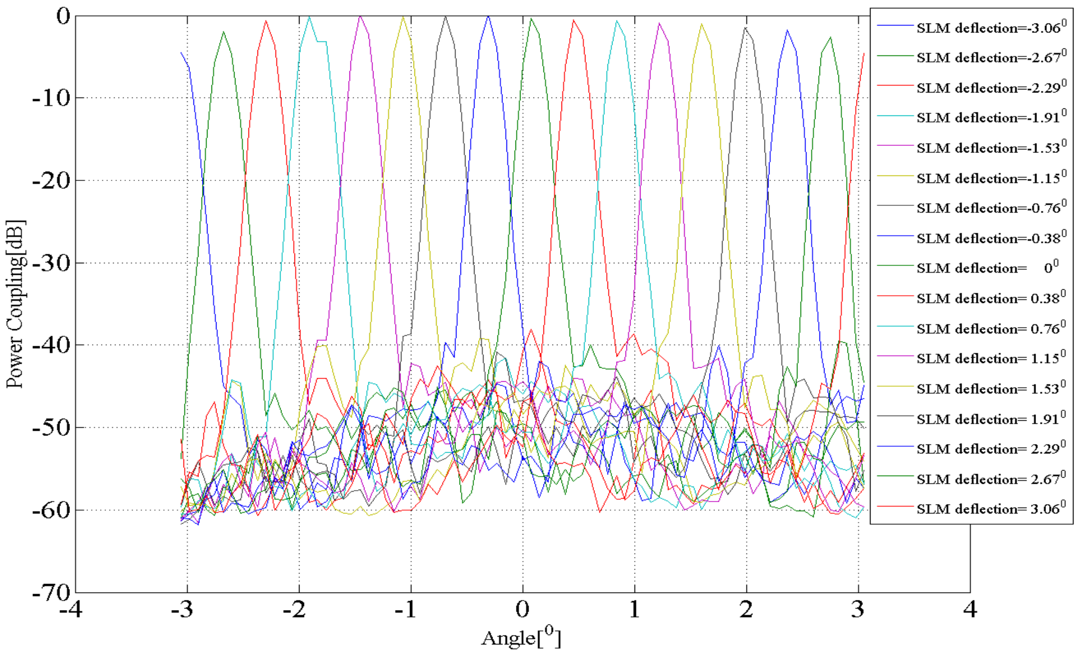

Fig 5.2.4.2: The diagonal tilt experiment.

The crosstalk was indeed reduced significantly as most the values were below 40 dB.

Modified setup

The physical and mode diameters of the I/O collimators are 4mm and 0.4mm respectively. Therefore, the minimal pitch, in the current setup, is 4mm which is 10·(2Δ). However, the typical pitch value in WSS system is 1.5· (2Δ) (40 dB criteria). Thus, the above setup is not a realistic representative, as the greater pitch achieves better results.
The setup (fig 5.2.4.3) was modified, for achieving the desired pitch, by using a beam splitter which folded the light. Thus, the input and output collimator were no longer in the same physical plane (both collimators are still in the effective front Fourier plane). Therefore, the minimal pitch value is no longer limited, unlike the previous setup. But we do get excess IL due to the double passing of the beam splitter (which is a system artifact here, and can be eliminated in a real system).

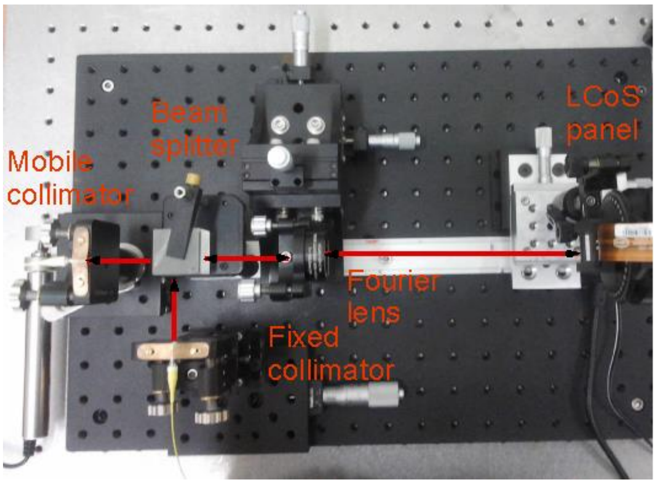

Fig 5.2.4.3: The modified setup

The output collimator was aligned with the optical axis and the input collimator was located 0.6mm (1.5·(2Δ)) below the optical axis.
The results of the diagonal tilt experiment in the modified setup are shown in the graphs 5.2.4.4. Unlike previous graphs the total insertion loss (instead of normalized results) is presented which is comprised of the following loss sources:

1. LCoS Reflection and setup loss (3.3dB)

2. Beam splitter loss (11dB)

3. Switching loss (according to the steering angle).

4. The source laser is not polarized. Therefore, half of the input power (3dB), the polarization element orthogonal to the required one is lost.

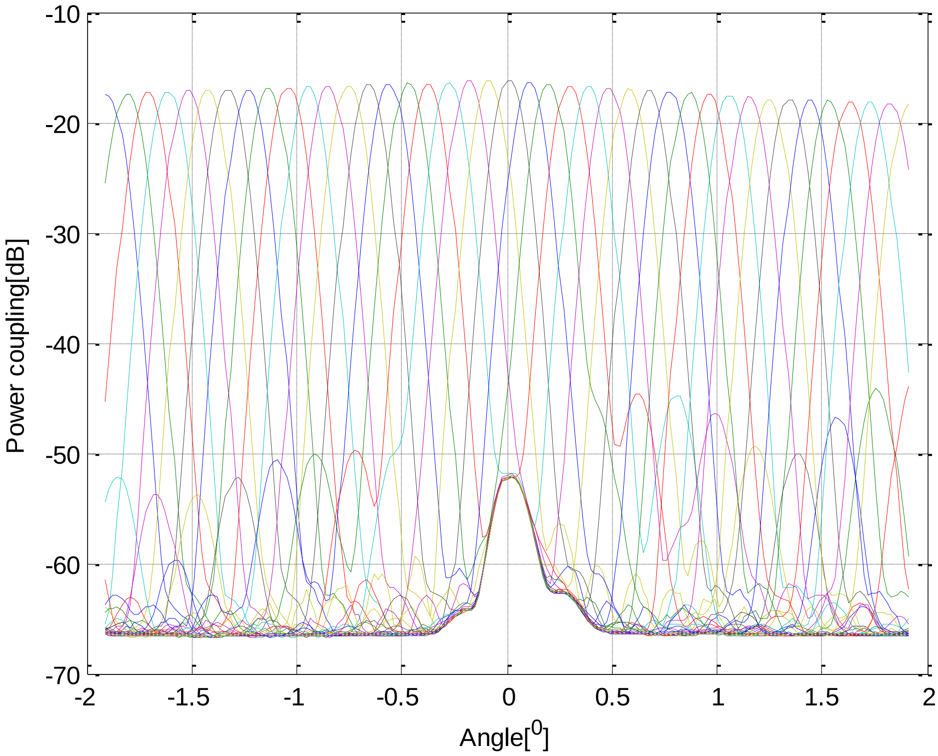

Fig 5.2.4.4: The diagonal tilt experiment conducted in the modified setup

The crosstalk was reduced (compared to the non-diagonal tilt experiment). Only the second diffraction order was prominent and yet its value is less or equal than -30 dB (normalized value) which is much better than the symmetrical case crosstalk values (less or equal than -15dB). It is important to emphasize that the peak in the zero angle is the orthogonal polarization source (not a diffraction order).

The effect of attenuation (required by switching applications) by the beam offset method was also examined using this setup. Holograms inflicting losses (relative to the non-attenuated state) of 3dB, 6dB, 9dB and 12dB were generated. The attenuation was implemented by upper and lower deflections in the vertical direction.

Representative curves of attenuation achieved by applying lower deflections in the vertical direction are shown in fig 5.2.4.5

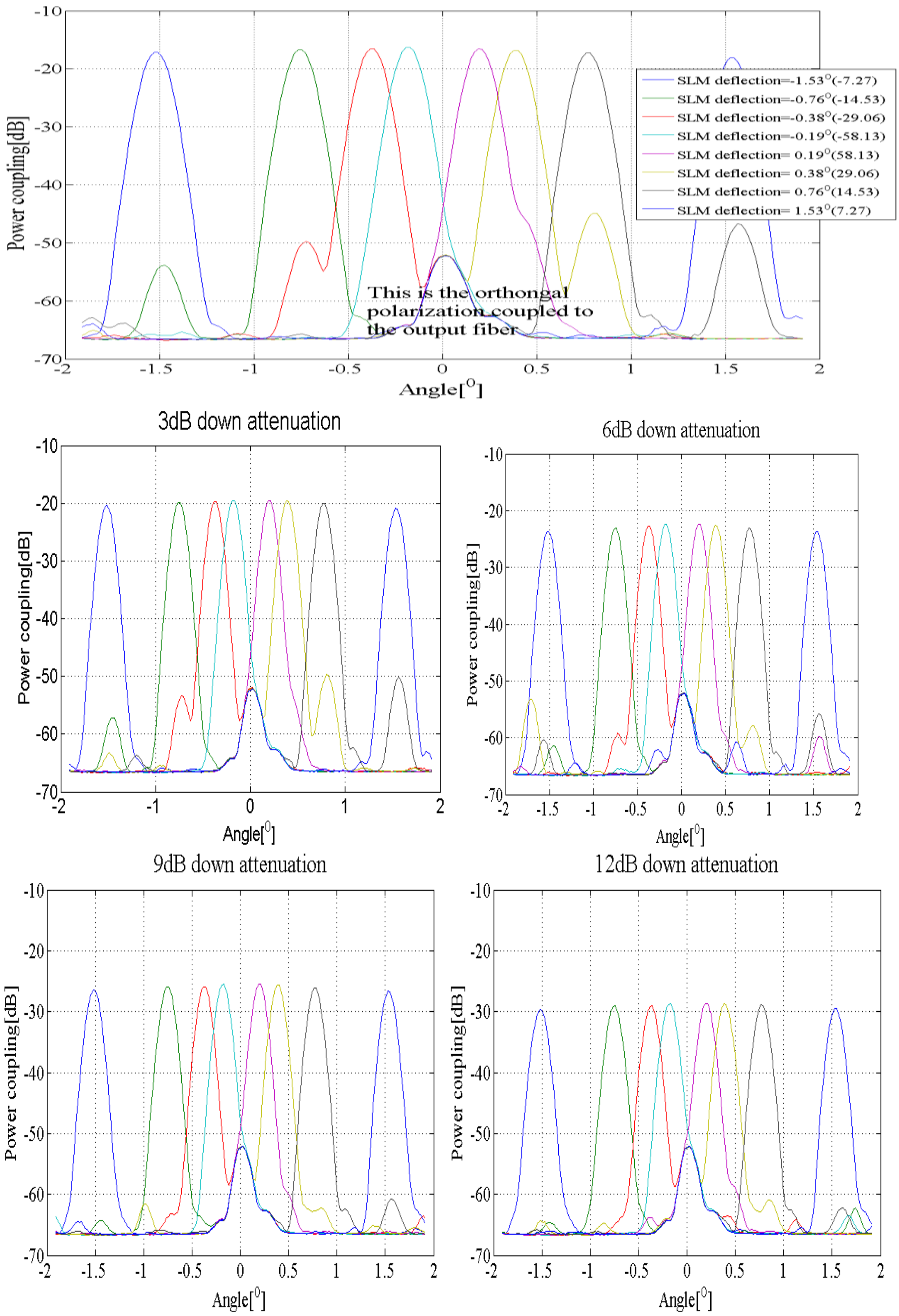

Fig 5.2.4.5: Power coupling vs. angle for no attenuation (top, the number in the brackets (legend) is LCoS period corresponding to the SLM deflection), 3dB, 6dB, 9dB and 12dB down attenuation

The crosstalk is reduced for the down deflection case because the overlapping, of 2nd diffraction order (The main crosstalk source) and the axis of output collimators, is reduced as depicted in fig 5.2.4.6 (top). However, the crosstalk is greater for the upper deflection case since the overlapping is increased fig 5.2.4.6(bottom).

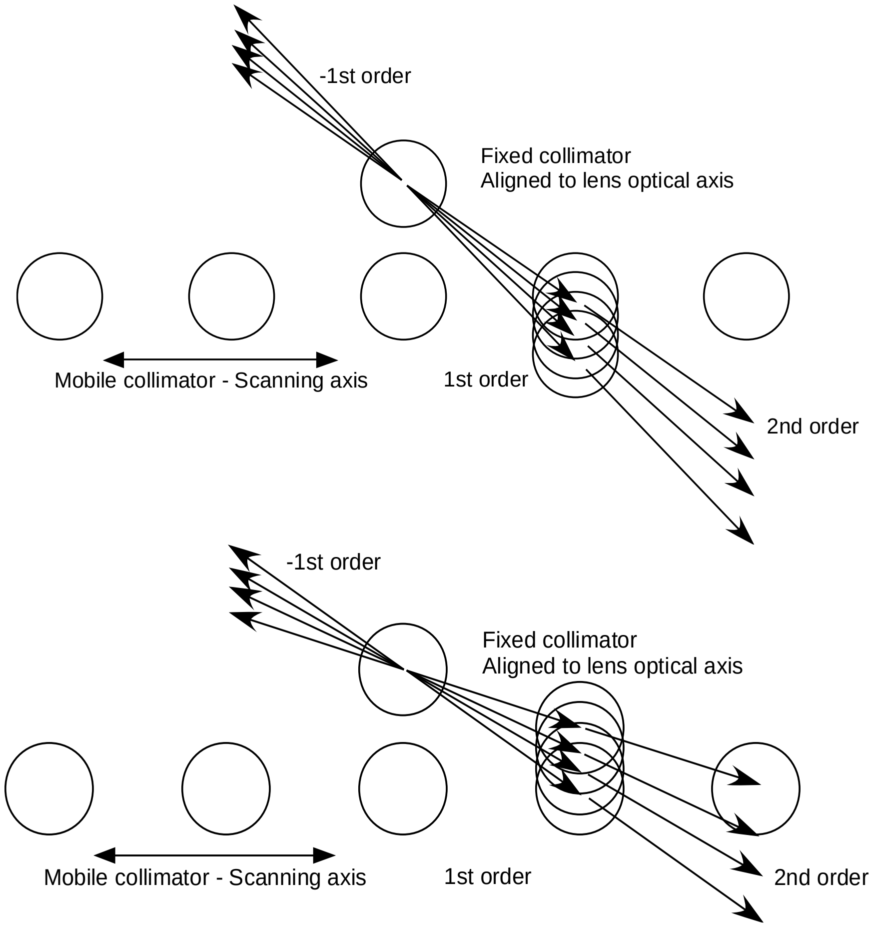

Fig 5.2.4.6: The effect of beam shifting downwards (top) and downwards (bottom) deflection on the diffraction order locations (main crosstalk source comes from the ±2 order)

The results of the up deflection (shown in fig 5.2.4.7) attenuation experiment indeed verify that the crosstalk worsens as expected. The 3rd (not only the 2nd) diffraction order also became prominent for some deflections.

It is important to emphasize that diagonal tilt inflicts deviation along the grating k-vector. Therefore, the peaks of the undesired diffraction orders do not coincide with peaks of the target orders which lead to a reduction of the crosstalk. It is clear that down deflection is the optimal method for implementing the attenuation mechanism for the collimators arrangement described in the current section, as higher orders do not couple to available ports. If detuning upwards, second order diffraction can exactly coincide with fiber port.

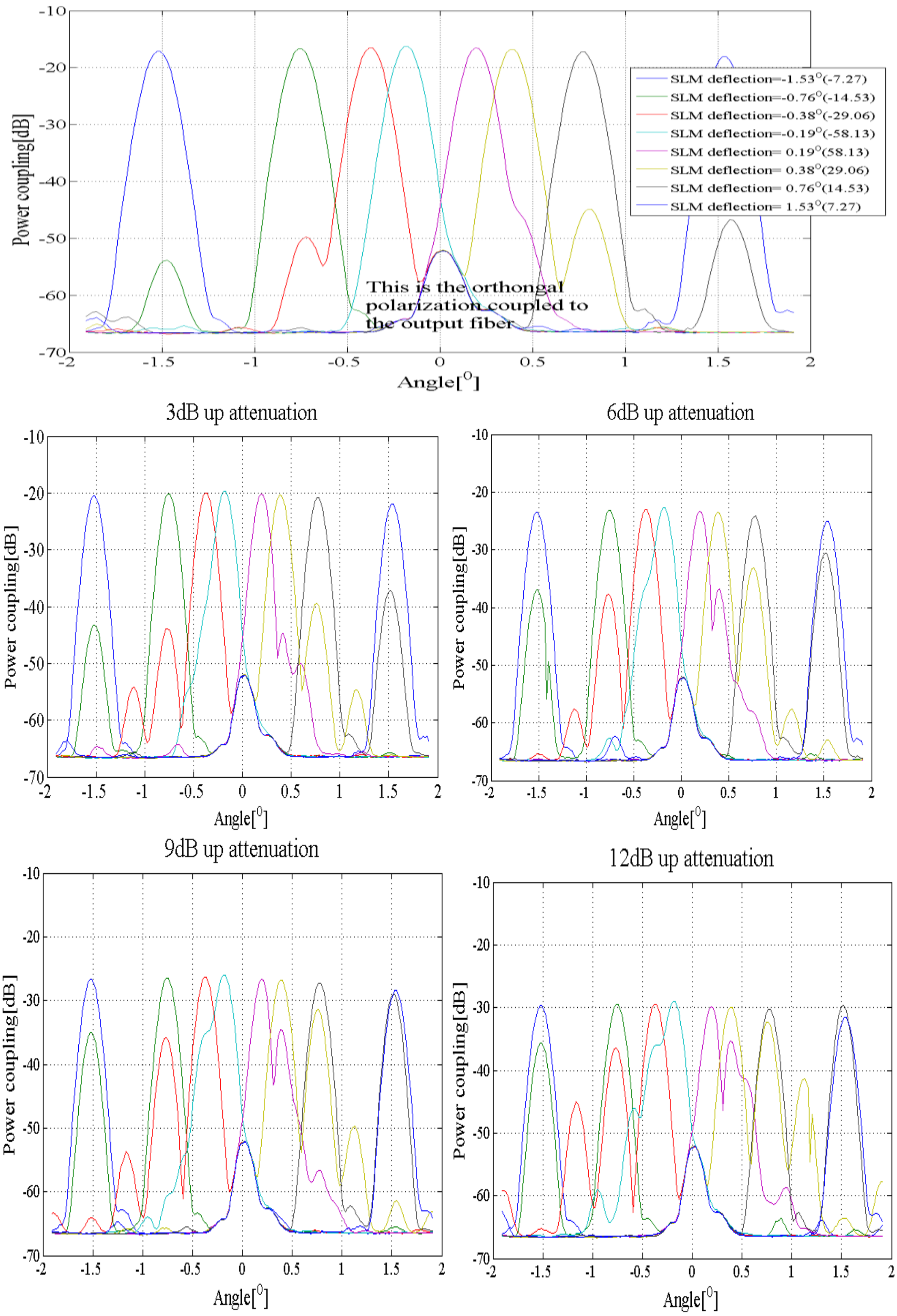

Fig 5.2.4.7: Power coupling vs. angle for no attenuation (top), 3dB, 6dB, 9dB and 12dB up attenuation

5.3 *Flicker*

The temporal response of the LCoS SLM was examined as well.
The power variation in diffraction (relative to the DC level) and frequency were measured by an oscilloscope (Fig 5.3.1) for different SLM deflections.

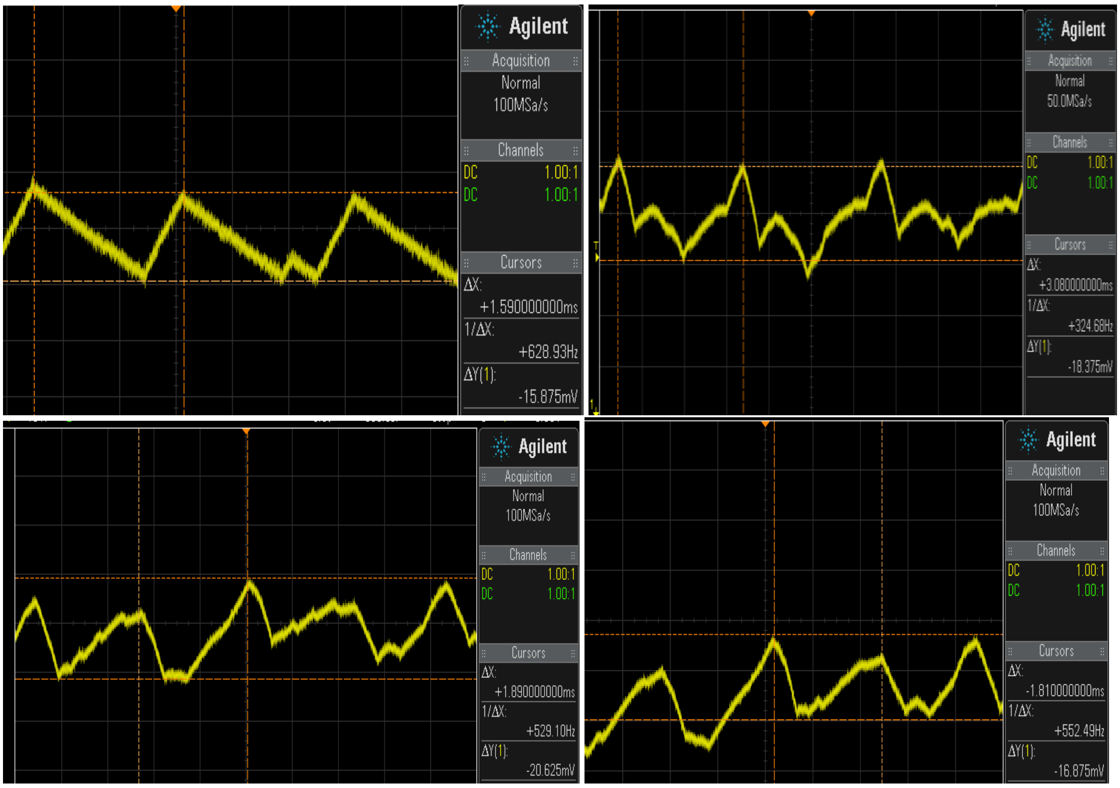

Fig 5.3.1: The temporal behavior of the LCoS for the following deflections: Top left: 0°. Top right: 0.19°. Bottom left: 0.38°. Bottom right: 0.57°

The table below summarizes the results:

Frequency[Hz]	Amplitude to DC level ratio[%]	Deflection[°]
628	0.48	0
324	0.7	0.19
529	0.93	0.38
552	0.72	0.57

1) The temporal response is quasi-periodic and the frequency is around 500 Hz.

2) The amplitude to DC level ratio is less than 1% for all applied SLM deflections. This corresponds to 0.05 dB in power variation.

5.4. Expected crosstalk performance of the switch

The performance of the switch is supposed to be better than contemporary commercial available LCoS SLM based switches.

There are two factors, in the switch, which help reducing crosstalk:

1) Collimator arrangement: The collimator are in the 2D array (as mentioned in section 4). Therefore, diagonal tilt is required for performing the switching. This proved (in section 5.2.4) to be an efficient tool in crosstalk reduction.
2) MEMS misalignment: The undesired diffraction orders are misaligned by the MEMS (in the output part). Therefore, not targeting the array (or targeting in high angle that reduces the power coupling of the undesired orders to the array)

6. Experiments

Proof of concept experiments are demonstrated in this section. The examined setup differs from the design in two elements:

1) LCoS SLM is used instead of MEMS. Therefore, this prototype can be tested only for one polarization because the LCoS SLM operates only on one polarization. The port count is limited as well because of the LCoS SLM physical aperture.

2) Collimator array: We use an available 19×19 collimator matrix (we use only small number of collimators) instead of the designed array. The horizontal pitch of this element is larger than the deigned which leads to higher LCoS SLM deflections (higher switching loss) and larger beam aperture.

The opto-mechanical design will be discussed firstly as it affects performance and then three experiments will be presented later: 1×k WSS (in order to understand the expected performance of the final design in terms of PDL (The MEMS LCoS is not used in this setup) and switching experiments with several input fibers.

6.1 Opto-mechanical design

Mechanical design is important part in every optical system design. The mechanics has to provide stability and ensuring that all optical elements are aligned well.

The Fourier lens is the reference element of the setup. Therefore, the types of the mechanical mounts, of the other elements, were designed according to Fourier lens. Especially the heights of the elements were affected.

Another important decision was about the degrees of freedom which will be enabled to every element.

The different mount types will be discussed briefly in the following sub sections.

6.1.1 Mechanical mounts- Diffraction grating to LCoS

The Mechanical design (fig 6.1.1.1) of the switching part (grating to LCoS SLM) will be discussed firstly because the rest of the setup was adjusted according to it

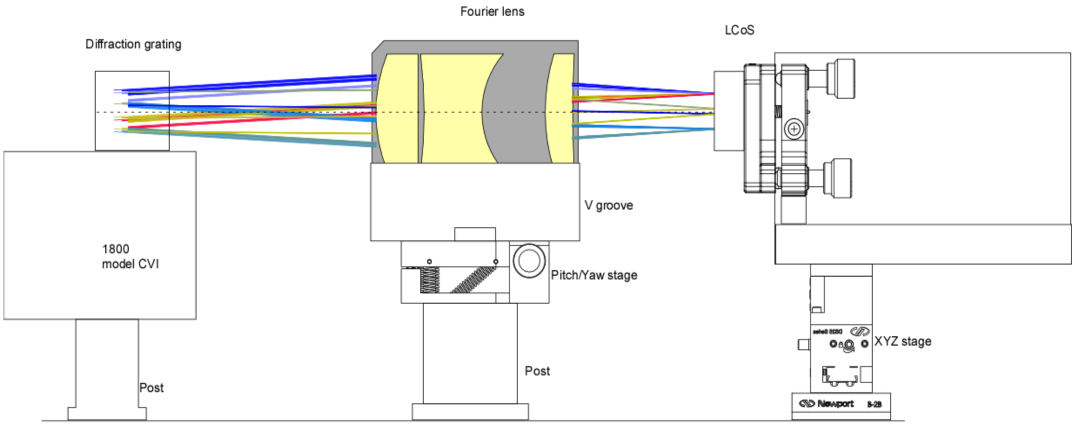

Fig 6.1.1.1 Mechanical mounting-Grating to LCoS

The Fourier lens is mounted to V groove (that was manufactured for us according a defined spec) on top of available commercial pitch/ yaw stage and post. Therefore, two rotational degrees of freedom are available to align the Fourier lens.

The diffraction grating is mounted on top CVI 1800 three axis stage and a post. Three rational degrees of freedom are available.

The LCoS SLM requires all three translational degrees of freedom because small deviations, caused by the other elements, can result in truncation. Therefore, we use XYZ stage and kinematic tip tilt (Thorlabs KM100B) for angular alignment. A mechanical ("L" shape) element for attaching the electronic board was manufactured for us according to a defined spec.

The mechanical design of the I/O optics will be presented in the next section

6.1.2 Mechanical design of input/output optics

Alignment of the input optics is important very important for performing the switching.

Misalignment of elements in this part can lead to significant performance degradation as it causes beam deviations or imaging failures due to distance errors in the cylindrical telescopes.

Firstly, the light beams need to be guided properly from Collimator array to the cylindrical optics through the LCoS(which substitutes the MEMS temporarily). Thus, the collimator will mounted on tip/tilt kinematic element (KM200B with slight adjustments) on top of XYZ stage as shown is fig 6.1.2.1. The LCoS mount was described in the previous section

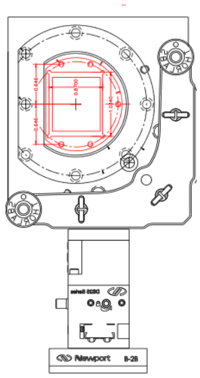

Fig 6.1.2.1 Collimator mount

The cylindrical optics (except one cylindrical lens) will be mounted on an aluminum bench. Side plates (with pins) are used for ensuring position, height and perpendicularity to the ground.

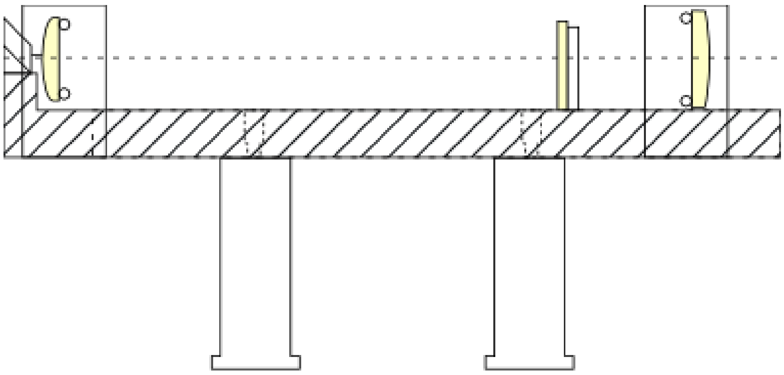

Fig 6.1.2.2. Cylindrical optics bench

The 30mm cylindrical lens is mounted independently due to higher sensitivity to angular deviations because of the short focal length. XYZ stage and kinematic cylindrical holder are used for mounting this lens

The top view of switch, with the cylindrical mounting mechanics incorporated, is shown in fig 6.1.2.3.

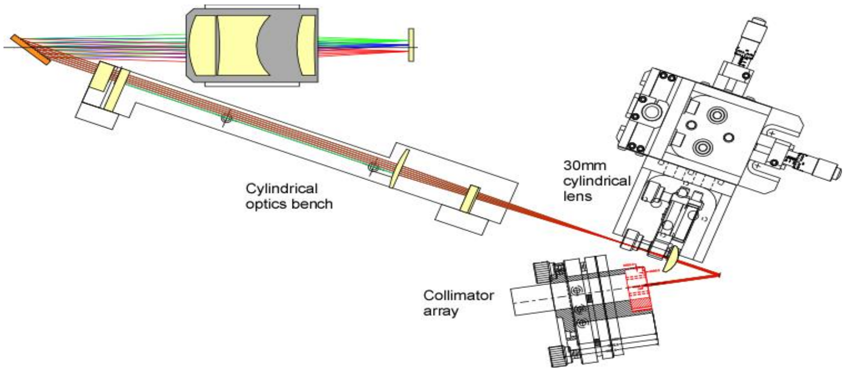

Fig 6.1.2.3 Top view

6.2 Conventional WSS experiment

The first experiment, for better understanding of the system's sensitivities, was of 1×9 WSS.

The experimental setup is shown in figure 6.2.1- Same system without the LCoS MEMS element. Therefore, the input signal can be separated only according to wavelength channel in the LCoS plane (in the Fourier plane).

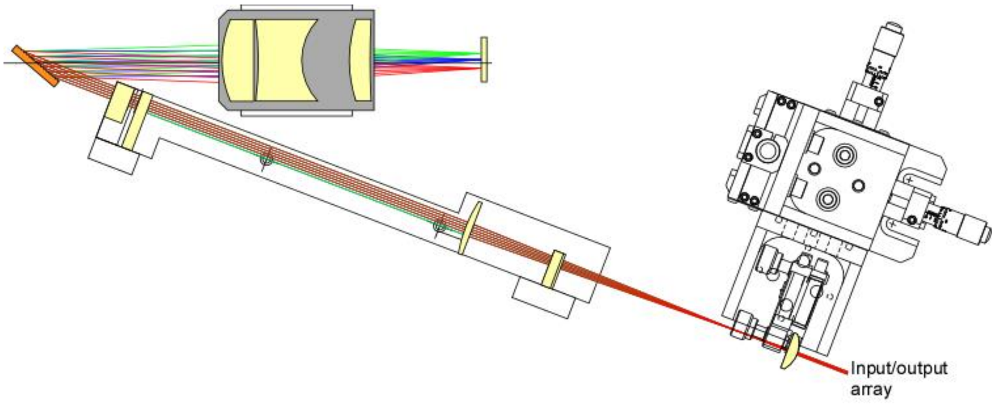

Fig 6.2.1 1×k WSS setup

This setup enables us to examine the performance in terms of PDL (which cannot be examined in the final experimental setup because LCoS SLM is used instead of MEMS and we are forced to discard one polarization), sensitivity of cylindrical optics alignment and Fourier lens alignment.
At first, the performance in terms of insertion Loss and PDL was very poor. The reason was angular misalignment between the 30mm cylindrical lens to other cylindrical lenses (placed on the cylindrical optics bench). Therefore, we positioned the 30mm cylindrical lens on 3 angles stage. This lead to dramatic performance improvement.

Port switching results are shown in graph below (port 5 is the input).

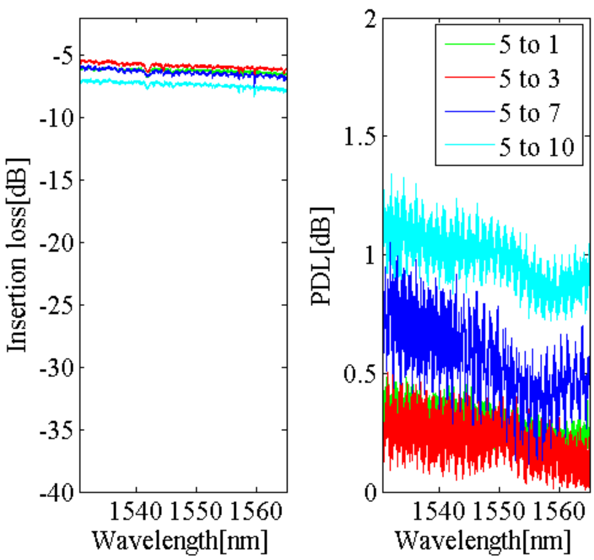

Fig 6.2.2 Insertion loss (left) and PDL (right) for certain switching configurations.

This performance is not far from Finisar's LCoS SLM based WSS (Appendix D). It can further improved if more sensitive 3 angles stage is used.

Example of wavelength switching is shown in figure 6.2.3. Certain wavelength channels were switched from port 5 to 1

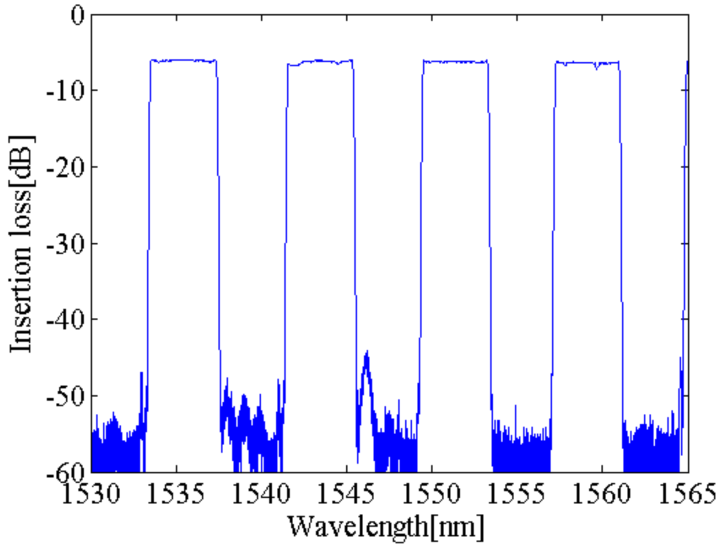

Fig 6.2.3 Spectral Switching

The performance in terms of crosstalk was examined as well. Typical result is shown in figure 6.2.4. Switching pattern to port3 was applied on the LCoS SLM and power was measured in port 9 (which corresponds to -2 diffraction order of this LCoS SLM pattern).

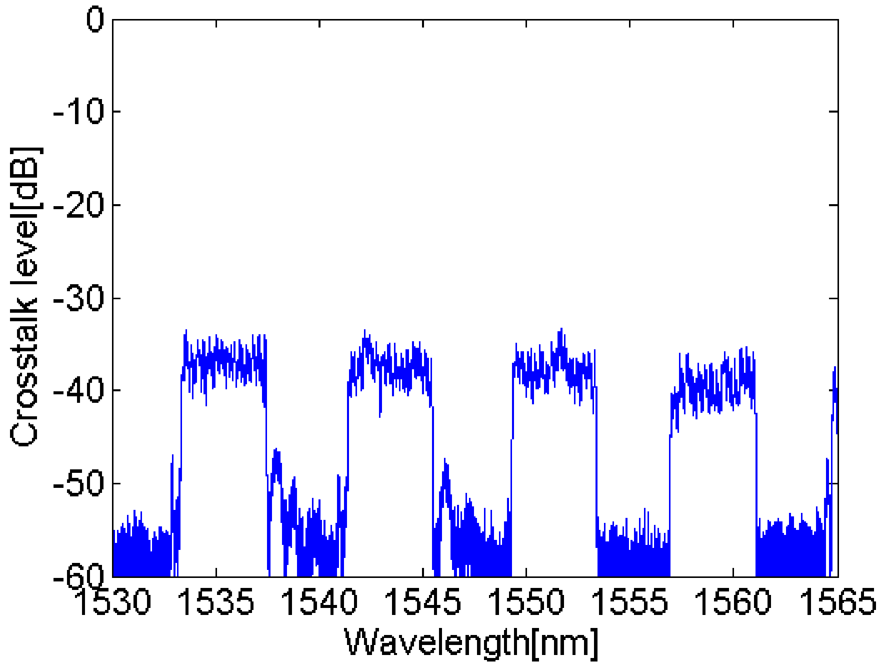

Fig 6.2.4 Crosstalk level

It is important to note that we used in this experiment high quality 1D collimator array

6.3 Proof of concept experiment

The first experimental setup, to demonstrate switching from multiple input ports, was 3×11 (three input ports and eleven output ports) WSS. This experiment included only one column of the collimator matrix (not the array used in the previous section).

The 2nd LCoS SLM (which will be replaced by MEMS in the final device) was inserted to the system. Unique beam deflection angle was applied per input port which enabled the spatial port separation in the Fourier plane LCoS SLM (as explained extensively in section 2).

The disadvantage of using 2nd LCoS SLM instead of MEMS is greater additional "zero state" loss and higher beam deflection loss (it is important to note that there is a double pass in the 2nd LCoS plane).

The three input ports were 5, 8(aligned with cylindrical optical axis) and11 (collimator 1 is the top and collimator 14 is the bottom). The deflection angles applied, by the MEMS LCoS, were -0.5°, 0° and 0.5° respectively which created a 3mm spatial separation between adjacent ports in the LCoS plane (The mode diameter in the LCoS plane was approximately 1.3-1.4mm).

The performance of representative switching configurations are shown in the graphs below.

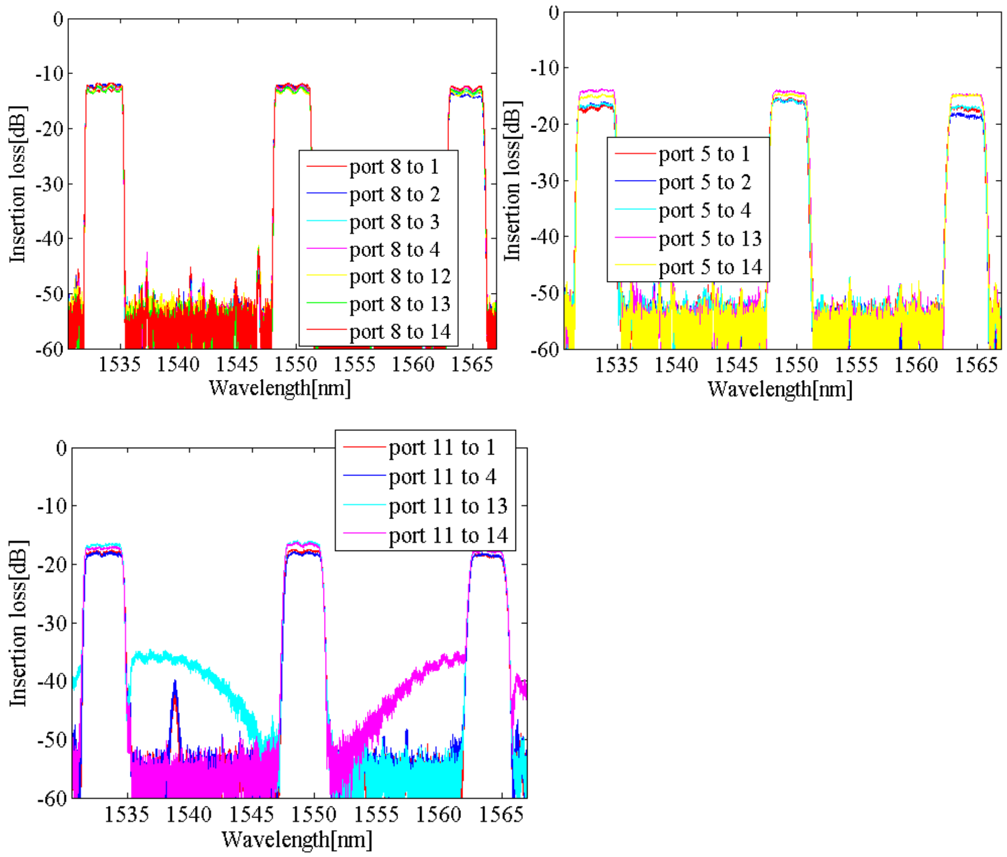

Fig 6.3.1 Switching from port 8(top left), 5(top right) and 11(bottom)

There is an amplitude modulation effect when the switching from port 8 because of low quality AR coating of the Holoeye LCoS SLM (which will not occur with

MEMS). The modulation amplitude is reduced when the switching is performed from ports 5 and 11 because the applied deflection angle is not zero.

The insertion loss for the input ports 5 and 11 is greater than for port 8 (no beam deflection is applied by MEMS LCoS) because of the beam deflection loss (in a double pass) inflicted by the MEMS LCoS.

This experiment demonstrated the concept of multi input port switching achieved by creating a spatially separated port/spectral grid in the Fourier plane spectral LCoS SLM. The performance will improve dramatically when MEMS will be used instead of the 2nd LCoS SLM and for better opto-mechanics that will improve the cylindrical lenses alignment.

6.4 Two column switching experiment (7x21 WSS)

This experiment tested the performance of 7×21 WSS in terms of insertion loss and crosstalk level. The ports were arranged in two columns of the fiber array (fig 6.4.1). All input ports were positioned in one column and the horizontal coordinates (of the horizontal cylindrical lenses) were 0.25 pitch (column one (input port are inside this column)) and 0.75 pitch (column2) because of switching and crosstalk considerations (described in section 5.4). It is important to note that collimator eight is aligned with vertical cylindrical optical axis.

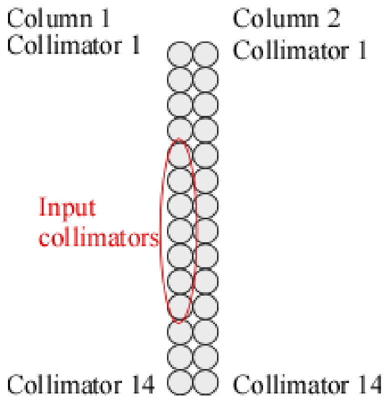

Fig 6.4.1 Collimator layout in this experiment

Switching configurations from several input to output ports (positioned in both columns) were sampled. It is important to emphasize that, unlike previous experiments, a serious beam deflection (about 2.4° (4.6 pixels per period)) was applied by the spectral LCoS SLM in the horizontal direction due to the fact that we used an available array with higher horizontal pitch than designed (the beam deflection will be smaller (≤2°, ≥5 pixels per period) when the designed array will be used). Therefore 2D phase pattern was applied on the LCoS SLM as shown in fig 6.4.2.

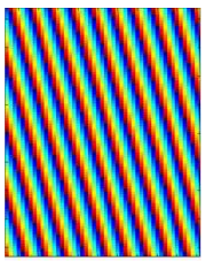

Fig 6.4.2 2D sawtooth phase pattern

The tested input ports were 7, 9, 10, 11 and 13 and the applied beam deflection by the MEMS LCoS were 1°, 0.4°, 0,° -0.4° and -1° respectively. This generates vertical layout, in the spectral LCoS SLM plane, in the coordinates 5.8mm, 2.3mm, 0mm, -2.3mm and -5.8mm respectively. The spatial separation, according to input port in the spectral plane, was verified by zero pi scan (appendix C)

6.4.1 Switching to column 1

The switching performance to output ports in column one is shown in this section. In the overall the loss value is stable per input port. There are certain cases with higher insertion loss than expected (which can be reduced with high tolerance opto-mechanics).

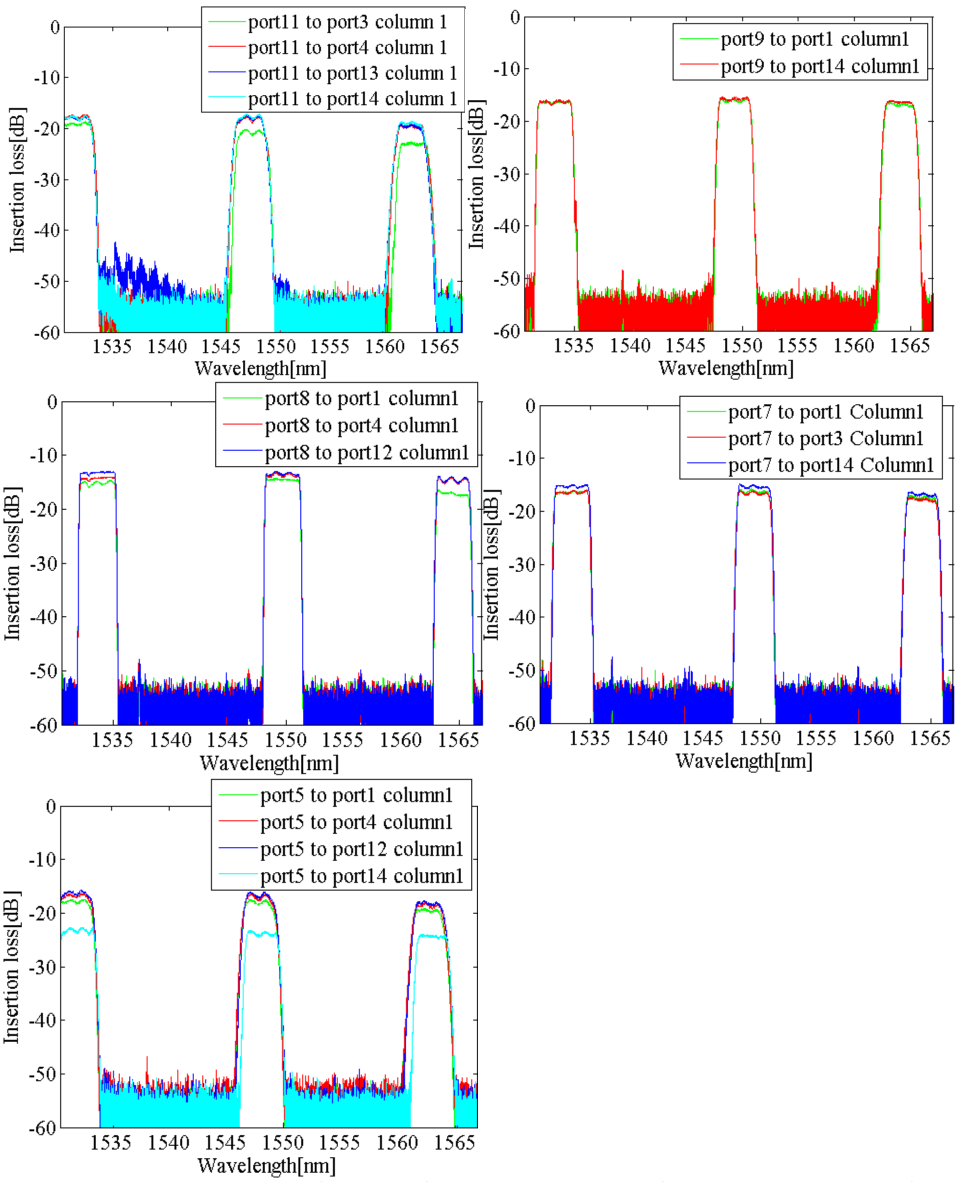

Fig 6.4.1.1 Column1 switching configurations from input ports 11(top left), 9(top right), 8(middle left), 7(middle right) and 5(bottom)

6.4.2 Switching to column 2

The switching performance to output ports in column 2 is shown in fig 6.4.2.1.

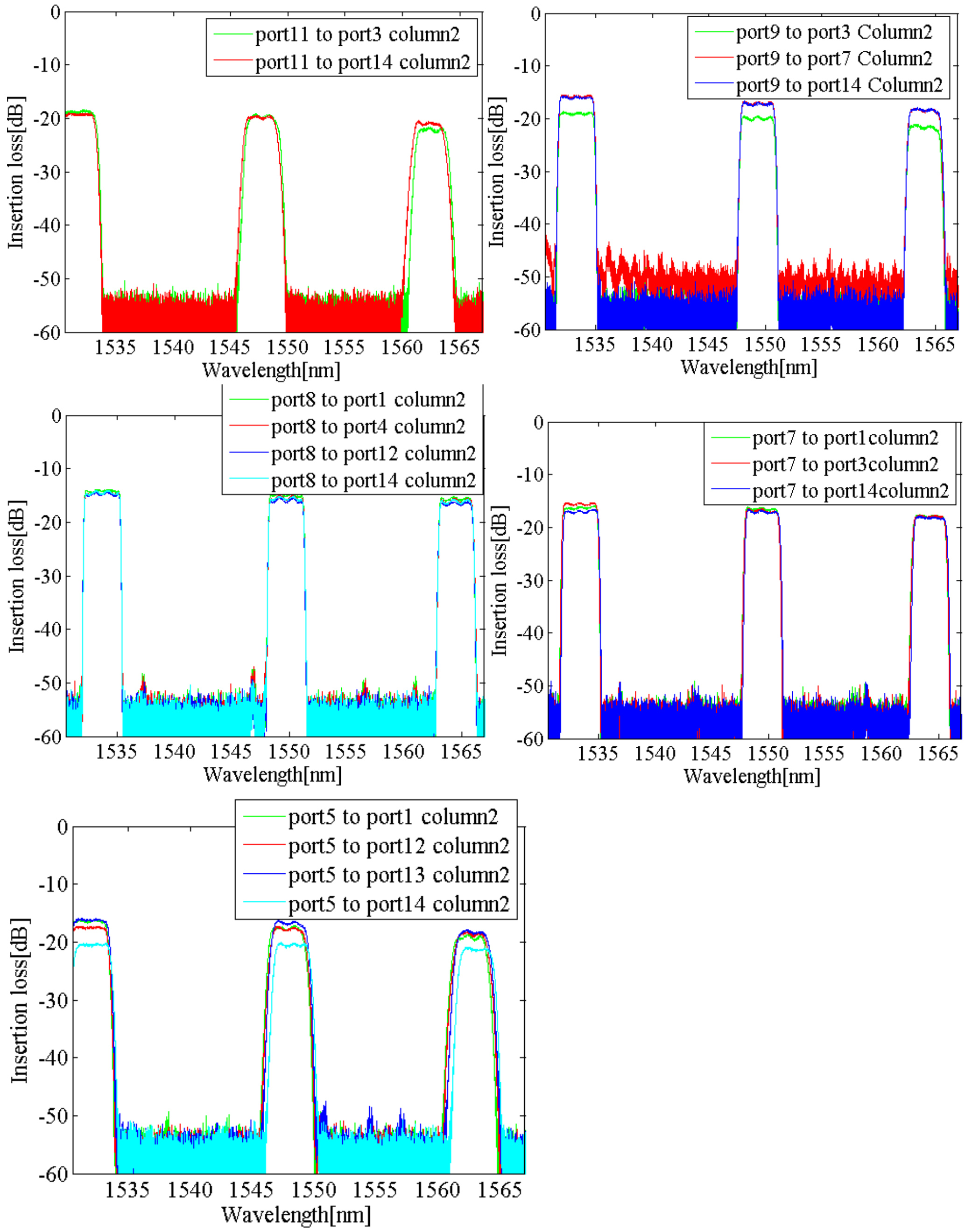

Fig 6.4.2.1 Column2 switching configurations from input ports 11(top left), 9(top right), 8(middle left), 7(middle right) and 5(bottom)

Tilt (about 0.2°) had to be applied in the horizontal direction (fig 6.4.2.2) by the MEMS LCoS for performance improvement (unlike the switching to column 1). This implies that a more sensitive opto-mechanics is required for better alignment of the horizontal telescope.

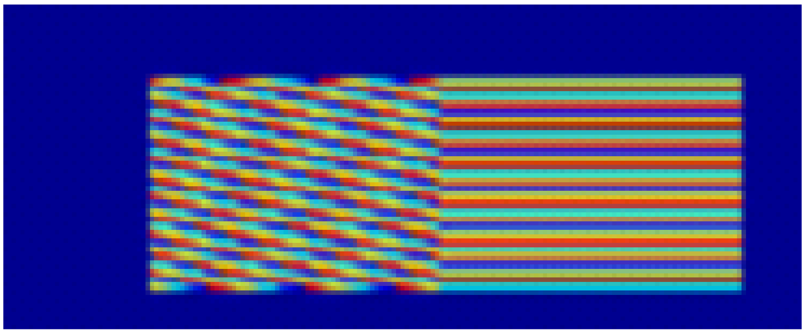

Fig 6.4.2.2. The input pattern (top) applies tilt in one direction while in output pattern tilt is applied also in orthogonal direction.

The switching, to output ports in the 2nd column, required to optimize locally the beam deflection (in the horizontal direction) applied on spectral bands (as expected by the Zemax simulation). The tilt variation was up to 0.4°, across the spectrum, to certain switching configurations.

It is important to note that there was indeed a horizontal shift of spectral components according to input port as expected (and described in sections 2.3 and 3.1.2).

6.4.3 Insertion loss analysis

The insertion loss (for different switching configurations) of the switch depends on the following parameters:

1) "Zero state" (when no phase applied) loss (of about 2dB per device) of both LCoS devices in the setup. It is important to note that anti-reflection coating performance of MEMS LCoS is degraded because the incidence angle is 15° (the anti-reflection coating is optimized for small angles of incidence according to research and development manager of Holoeye). The total "zero state" loss of the three devices is greater or equal to 6dB

2) Switching loss (which depends on the switching angle as extensively discussed in section 5) of both LCoS devices (one and double pass in the spectral and MEMS LCoS devices respectively). The minimal Switching loss of the spectral LCoS is 2.5dB (not including the vertical tilt) because for all configurations 2.4° (4.6 pixels per period horizontal tilt is applied.

3) Efficiency of the diffraction grating, which is about 85% (for the lithrow configuration) according to the manufacturer. Therefore, the loss inflicted by double pass in the grating is greater or equal to 1.5dB.

4) The insertion loss of the collimators in the array which is about 2-3dB in a double pass according to characterization experiment. This is a vintage 2000 fiber array. Modern fiber array achieve 1dB loss in a double pass.

5) Pointing error of collimators in array which cause misalignment that leads to additional coupling loss. We know, according to characterization experiments that parallelism of the collimators is worse than modern arrays.

6) The loss inflicted by the Fresnel reflectance from the double pass in the Fourier lenses (99.5% per lens according to manufacturer), cylindrical lenses (99% per lens according to Thorlabs) and PBS (95% transmission according to manufacturer). Therefore, the expected loss contribution of Fresnel reflectance is between 1-2 dB.

7) Optical aberrations- The expected nominal loss is 1 dB, but optical tolerances add at least 1 dB more.

The expected "zero state" (including the 2.4° horizontal tilt applied for all switching configurations) is about 13dB. This value is indeed not far from the performance when the switching is done from port 8.

The switching loss for other input ports is higher (than for port 8) because of the beam deflection loss inflicted by MEMS LCoS. The additional "zero state" loss when switching from ports 7 and 9 (0.4° beam deflection) is about 1dB (0.5dB per pass) and for ports 11 and 5(1° beam deflection) the additional loss is supposed to be about 2-2.5dB (1dB per pass).

The actual loss values, that added (to most sampled configurations) to port groups 5, 11 and 7, 9, were 3dB and 2dB respectively.

There were configurations that the loss was higher than expected. According to Zemax angular misalignment of the cylindrical telescopes can increase the switching loss. This factor can be improved in the next generation of the prototype which will include opto-mechanics that will ensure high alignment tolerance of the cylindrical lenses. This will result in reduction of optical aberrations

The problematic configurations were from ports 5 and 11 to output ports 14 and 1 respectively.

In the overall this experiment proved that two column N×M wavelength selective switching can be performed.

<u>Conclusions regarding the final setup</u>

The insertion loss in the final setup will better than, in this prototype, because of three reasons:

1) The MEMS, which will be used instead of the input LCoS SLM, will reduce the insertion loss to up more than 6 dB for certain configurations.
2) Collimator array with better degree of parallelism and smaller horizontal pitch .The horizontal tilt will be smaller which will lead to lower loss. The insertion of loss of the next generation collimator array will be about 1-1.5dB better in a double pass.
3) High tolerance opto mechanical alignment of the cylindrical lenses will lead to reduction of optical aberrations.
4) The fill factor, of the spectral LCoS SLM which will be used in the next generation prototype, will be higher. This will lead to 1dB improvement of the insertion loss.

6.4.4 Crosstalk

The performance in terms of crosstalk was examined as well in this experiment. The patterns of several switching configurations were applied on the LCoS SLM and the power in the other output ports (not the switching destination) was measured.

There are two main sources of crosstalk in an LCoS SLM based switch: Undesired diffraction orders and overlapping of power from adjacent ports.

The examined configurations sample the range of beam deflections applied by the LCoS SLM.

The first configuration to be examined is from port 9 to port 7 in column 2 (fig 6.4.4.1). The required tilt angle, in the vertical direction, is relatively small (0.2°, 51 pixels per period) and the beam deflection in the horizontal direction ranges from 2.15° (5.1 pixels per period) to 2.25° (4.9 pixels period) across the spectrum

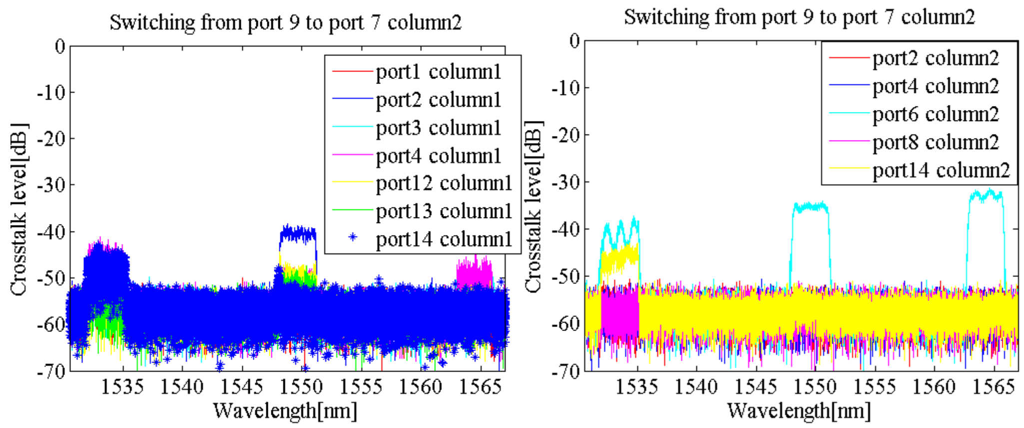

Fig 6.4.4.1 Crosstalk measurement for switching configuration 9 to 7 column 2

The highest crosstalk value was measured in port 6 in column 2, which is the adjacent fiber to the destination port. The contribution of the LCoS SLM diffraction orders is relatively small for this case (less than -40dB).

The switching configuration from port 11 to port 3 (fig 6.4.4.2) is an example for a mid-range deflection (0.8°, 14.3 pixels per period) in the vertical axis. The horizontal tilt is 2.3° (4.8 pixels per period)

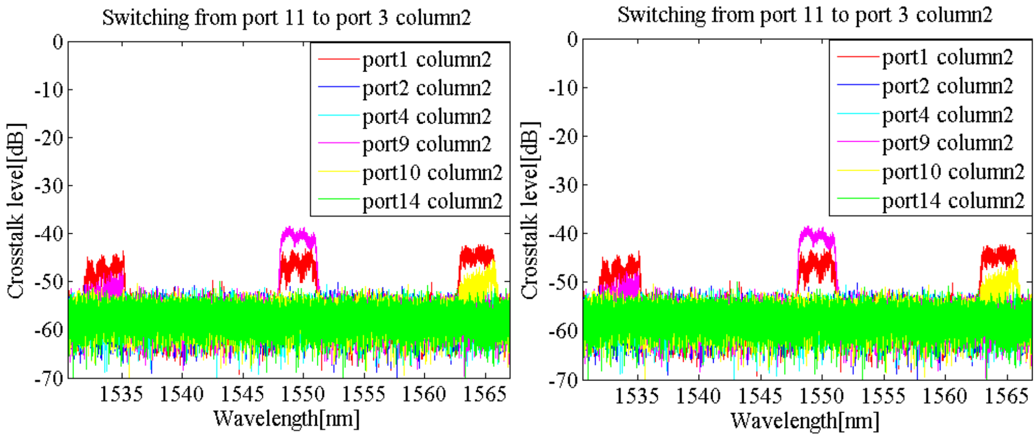

Fig 6.4.4.2 Crosstalk measurement for switching configuration 11 to 3 column 2

The main contribution to crosstalk was from the diffraction orders. However, the overall crosstalk was small (less than -35dB).

The next configuration represents the crosstalk performance for high beam deflections. The switching is performed from port 5 to port 1. The vertical deflection angle is 1.3° (8.5 pixels per period). The horizontal deflection varied from 2.15° to 2.25°

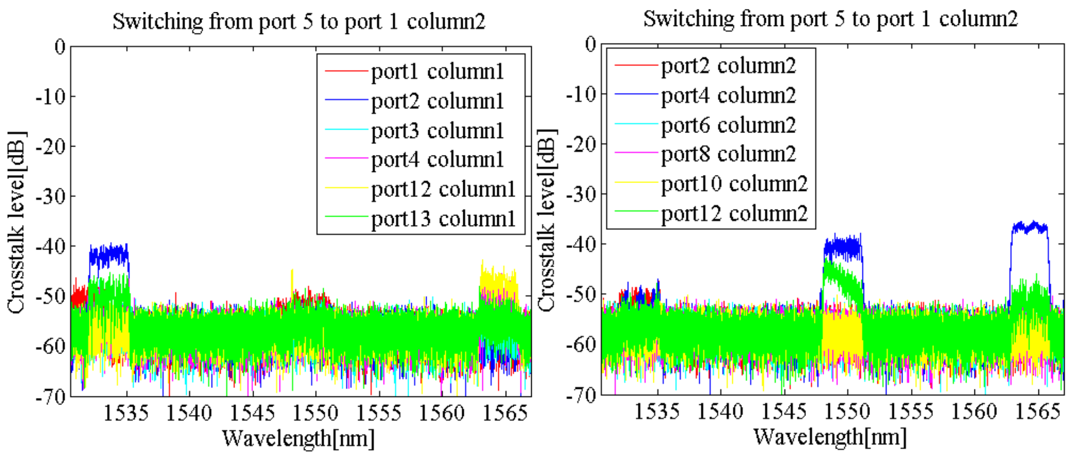

Fig 6.4.4.3 Crosstalk measurement for switching configuration 5 to 1 column 2

The main contribution to the crosstalk was from the long wavelength band in the adjacent port (4). The effect of diffraction orders was again less significant.

Generally, the crosstalk performance, of the other sampled switching configurations, was similar. However, there was one configuration in which the crosstalk was relatively high. It is important to note that again the effect of the diffraction orders were minor.

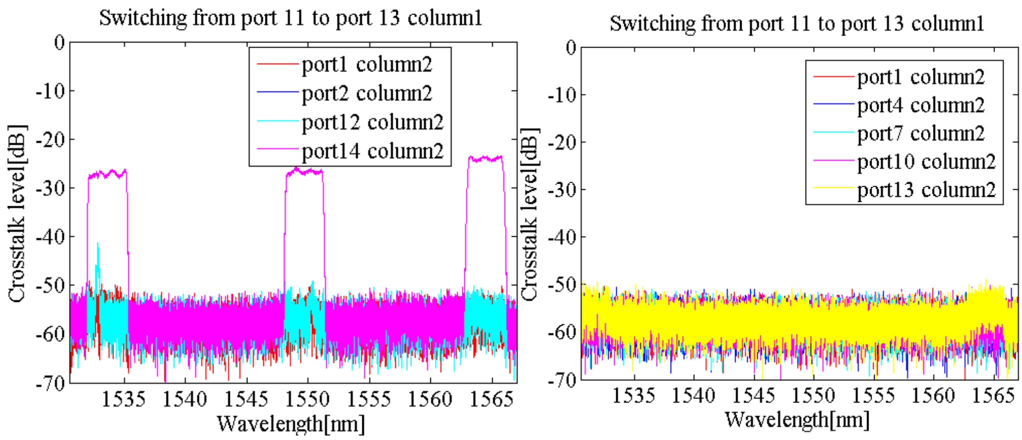

Fig 6.4.4.4 Crosstalk measurement for switching configuration 11 to 13 column 1

Conclusions

The collimator array arrangement (one column at 0.25 pitch and the other at -0.75 pitch) proved to be a useful tool in the reduction of crosstalk caused by the undesired diffraction orders of the LCoS sawthooth pattern. The main crosstalk source was overlapping Gaussians from adjacent ports (which was less than -30dB for almost all the examined cases). Which can be improved with more accurate array and cylindrical optics.

7. Conclusions

A novel approach was presented in this work for N×M wavelength selective switch device that would help in reducing the architectural complexity of the ROADM nodes.

The design, of the N×M WSS, was based on spatial separation of light beams according to input port and wavelength channel on a dynamic steering array (LCoS SLM). Which was extensively characterized in order to understand the switching capabilities and limitations.

We demonstrated wavelength selective switching from multiple input ports to multiple output ports in an initial prototype.

The performance in the final device will be better as the MEMS will replace the input LCoS SLM and better collimator array (as was designed) will be used. Expected insertion loss improvement of up to 9dB for the edge input ports.

8. Appendix A: Zemax software for optical design [9]

The software that was used for system and optical design, in this project, was Zemax. This software is capable of simulating geometrical ray tracing in optical systems and has a very important feature of Physical Optics Propagation (POP).

The POP analysis is based on Fresnel propagation and angular spectrum algorithms. It is a useful application for calculating power coupling in the fiber plane as the geometrical analysis ignores effects of physical optics that are critical for a design of optical communication device

9. Appendix B: N×N WSXC

The Fourier lens was designed firstly for a cross connect switch with N input fibers and N output fibers. As the optical requirements, for this project and N×N WSXC, are similar we decided to use the 120mm Fourier lens for the 8×24 WSS as well.

The port count (N) of the designed switch was ten (it is important to note that same fibers were used for input and output). The multi input and output port switching was achieved by creating spatial separation according to input port and wavelength channel on the LCoS SLM and double pass in the spectral plane.

We will mainly concentrate on the diffraction grating to diffraction grating propagation as the switching occurs in this part. The following design description is only conceptual. The fact that the same collimators are used for input and output is ignored and in the final design one grating is used instead of two and switches 1 and 2 (later will be described) are implemented by one LCoS SLM.

Firstly, the collimator plane is imaged in the switching direction and expanded in the spectral direction by two cylindrical telescopes. Therefore, N elliptical spots (which are spatially separated according to input fiber) are incident on the diffraction grating.

The switching process (in the ports direction) is shown in figure 9.1. The light beams, which are spatially separated according to input fiber on the diffraction grating, are directed to output grating (to coordinates assigned for the desired output port).

The light beams are separated according to input port and wavelength channel on dynamic steering element (switch1). A tilter is assigned per input port which induce unique beam deflection. Therefore, the light beams are angularly separated according to input port. The Fourier lens transforms it into a spatial separation according to input port on switch1. In the orthogonal, the Fourier lens transforms the angular dispersion (after the light beams are being diffracted by the grating) to spatial dispersion (fig 9.2).

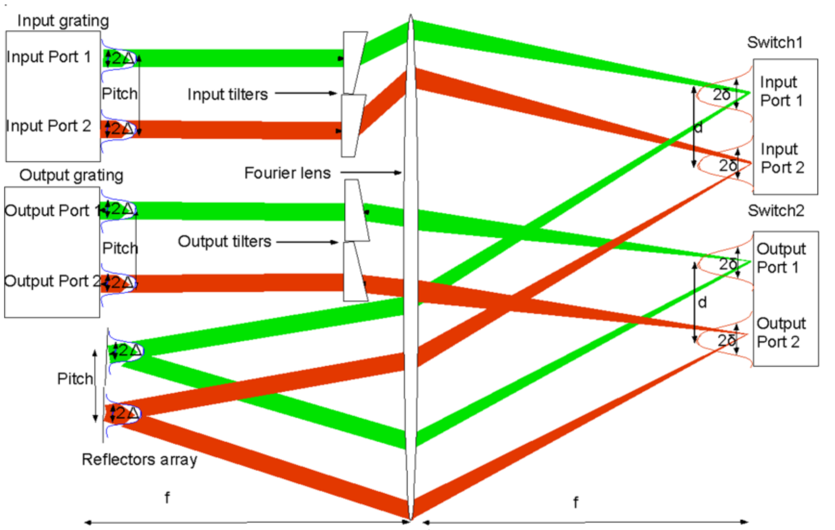

Fig 9.1: Grating to grating switching example for 2 ports system: Gaussian beams (mode diameter Δ) are steered from the ports of the input diffraction grating to the desired output port in the output grating. The colors represent switching configurations

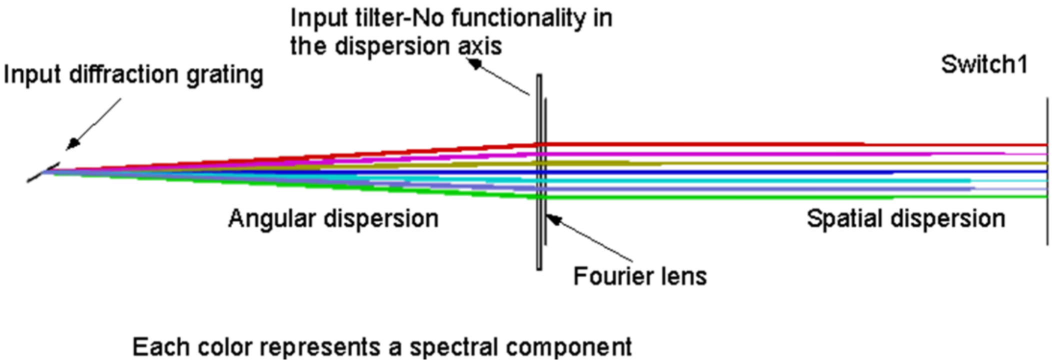

Fig 9.2: The light diffracted from the diffraction granting is angularly separated. Therefore each spectral element is imaged by the Fourier lens to a distinct coordinate in the horizontal axis of switch 1.

The beam layout in switch one is shown in fig 9.3. The spatial separation according to input port and spectral channel enables to apply multi-port wavelength independent switching

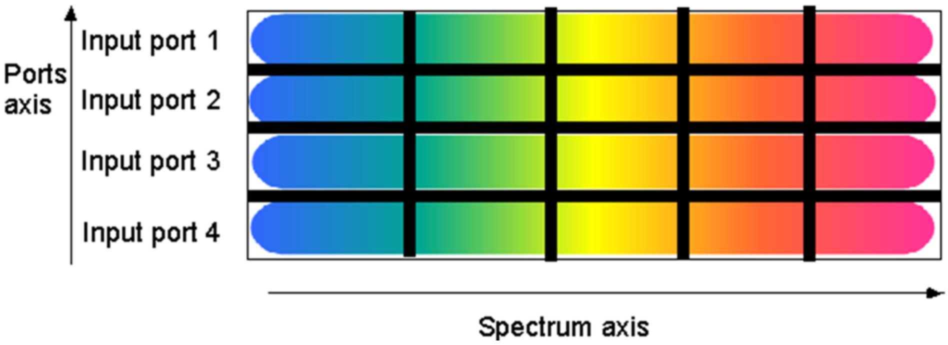

Fig 9.3 Switch 1 view: The signals in the back Fourier plane are separated according to the input ports and the spectral channels.

The actual switching occurs in the propagation from switch1 to switch2. The light beams are routed from the compatible input ports in switch1 to the compatible output ports in switch2 according to the desired switching configuration. An example, of this part for 4×4 WSXC, is shown in fig 9.4.

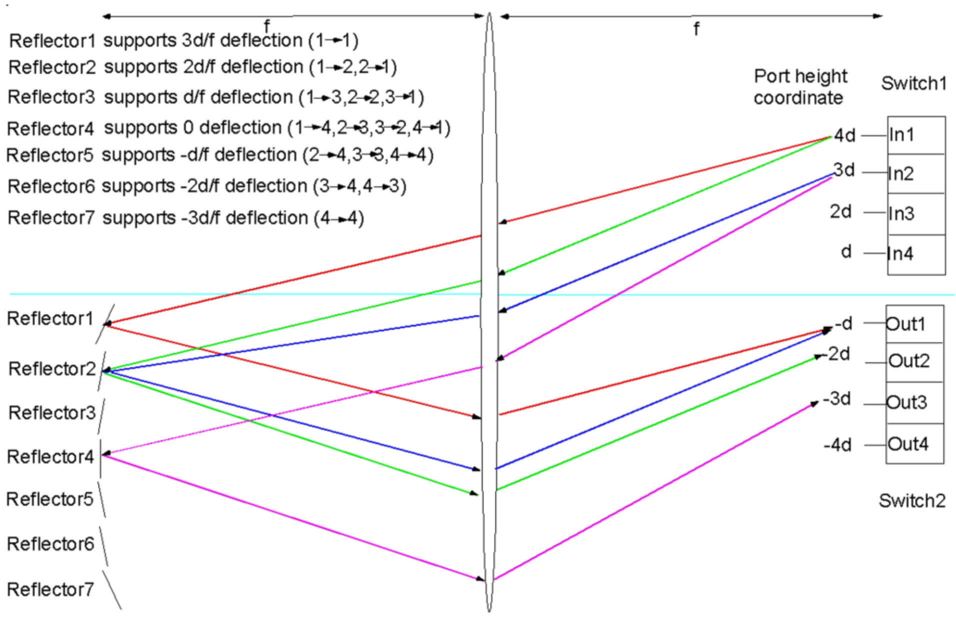

Fig 9.4. The supported switching configuration by the reflectors array of 4×4 WSXC-For each reflector the deflection value and the supported routing combinations (input to output).Each color represents a switching combination.

The light beam is routed by switch 1 to a reflector of port selector array. This reflector applies tilt that directs the light to the compatible output port in switch2. It is important to note that the port selector array is comprised of reflectors which apply fixed tilts.

For example, the switching configuration from Input port1 to output port1 requires a tilt of 3d/f (d is the pitch in the Fourier plane and f is the focal length). Therefore, switch1 applies local tilt (in the area of port in port 1) which direct it to reflector 1 which deflects the beam to compatible coordinate of output1 in switch2. If the required switching configuration is from input 1 to output 2 then switch 1 will steer the beam to reflector2. The beam layout, of switches 1 and 2, is shown in figure 9.5.

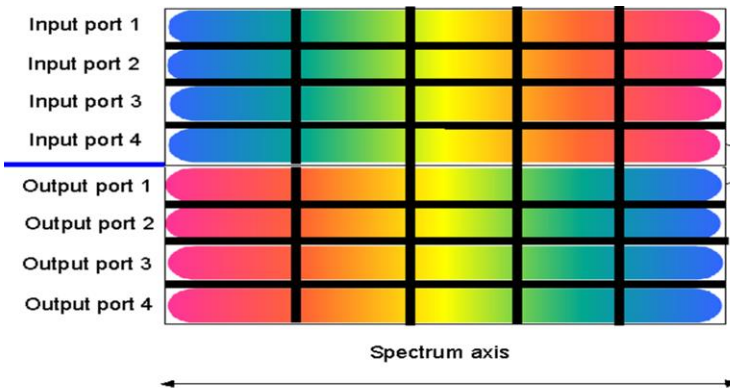

Fig 9.5. Beam layout of switch1 (top) and switch2 (bottom). The light beams are separated according to input or output port and spectral channel

The last part of the switching process is the propagation from switch 2 to the compatible coordinates of the output ports of the output diffraction grating (fig 9.6). Switch2 applies tilt which routes the ligh beams to the output tilters (tilter is assigned per output port) which realign the beams before propogating to the diffraction grating

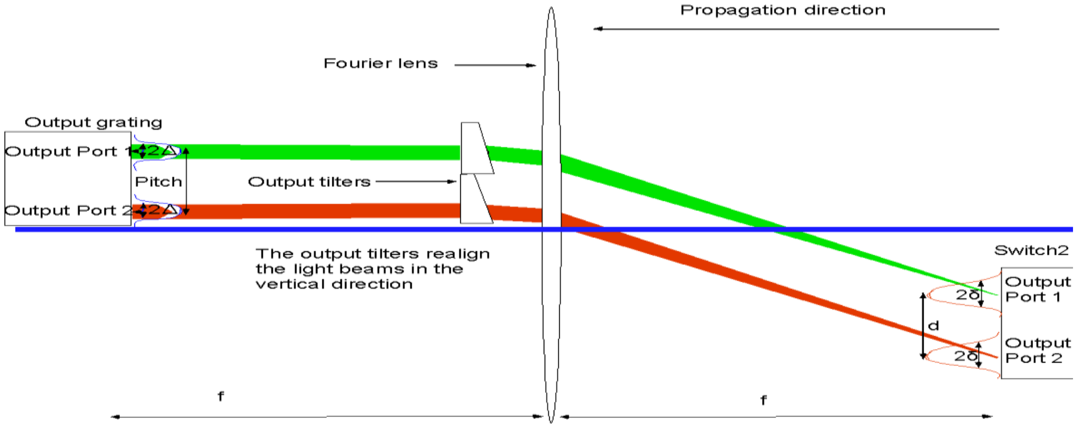

Fig 9.6. The light is being redirected to the output diffraction grating from Switch 2

The spectral elements are focus into one beam in the diffraction grating (in the spectral view). The grating plane is imaged by the cylindrical optics to collimator plane which couple them to the fibers.

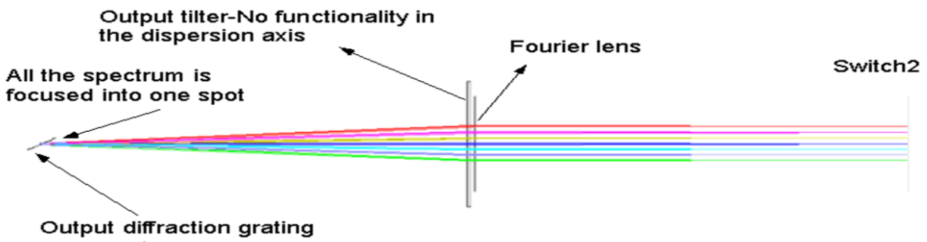

Fig 9.7. The wavelength channels are imaged to the one spot on the diffraction grating.

<u>Disadvantage of N×N WSXC based node [1]</u>

The drawback of the WSXC is its sensitivity to failures; if the switch malfunctions Or needs to be replaced, then all the WDM traffic flowing on the *N* fibers is halted. Therefore, 8×24 WSS based node is less sensitive as failure will affects only locally.

10. Appendix C: Zero-PI scan technique

Useful technique for finding the center of Gaussian spot on an LCoS SLM device is the Zero-PI scan.

Phase pattern of step function ($\varphi(x)$), with upper phase level π, is applied on the LCoS. The transition coordinate (between 0 and π) is changed dynamically by the user. Destructive interference occurs when the transition point is aligned with the center of the Gaussian ($G(x)$). The calculation, which shows the dependence of power (I) in the transition point x', is shown below. Therefore, the minimum of the intensity occurs in the center of spot (fig 1).

$$I=\int_{-\infty}^{\infty}G(x)\Phi(x-x')G(x)dx$$

$$=\left(\frac{2}{\pi w_0^2}\right)^{1/2}\int_{-\infty}^{\infty}\exp\left[-\frac{x^2}{w_0^2}\right]\exp\left[i\pi\cdot Step(x-x')\right]\exp\left[-\frac{x^2}{w_0^2}\right]dx$$

$$=\left(\frac{2}{\pi w_0^2}\right)^{1/2}\left[-\int_{-\infty}^{x'}\exp\left[-\frac{2x^2}{w_0^2}\right]dx+\int_{x'}^{\infty}\exp\left[-\frac{2x^2}{w_0^2}\right]dx\right]$$

$$=\left[\left(\frac{2}{\pi w_0^2}\right)^{1/2}\int_{x'}^{\infty}\exp\left[-\frac{2x^2}{w_0^2}\right]dx-\left(1-\left(\frac{2}{\pi w_0^2}\right)^{1/2}\int_{x'}^{\infty}\exp\left[-\frac{2x^2}{w_0^2}\right]dx\right)\right]=2\left(\frac{2}{\pi w_0^2}\right)^{1/2}\int_{x'}^{\infty}\exp\left[-\frac{2x^2}{w_0^2}\right]dx-1$$

$$\xrightarrow[y=\frac{\sqrt{2}}{w_0}x,\ dy=\frac{\sqrt{2}}{w_0}dx,\ x'\to\frac{x'\sqrt{2}}{w_0}]{}2\left(\frac{2}{\pi w_0^2}\right)^{1/2}\frac{w_0}{\sqrt{2}}\int_{\frac{x'\sqrt{2}}{w_0}}^{\infty}\exp\left[-y^2\right]dy-1$$

$$=\frac{2}{\sqrt{\pi}}\int_{\frac{x'\sqrt{2}}{w_0}}^{\infty}\exp\left[-y^2\right]dy-1=Erfc\left[\frac{x'\sqrt{2}}{w_0}\right]-1$$

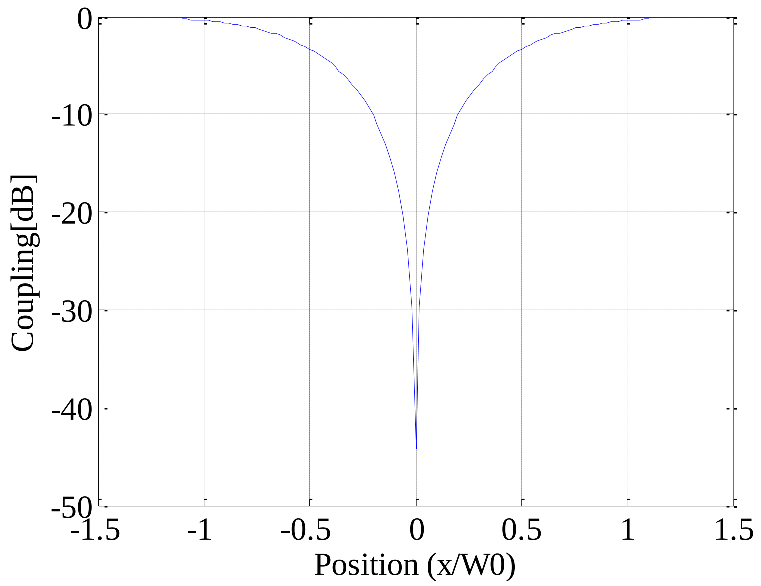

Fig 1. Zero-pi scan for finding spot center (x is the transition point coordinate between zero and π

11. Appendix D –Finisar's based LCoS WSS spec

The performance spec, of Finisar's LCoS based WSS, is shown in the figure below

OPTICAL PERFORMANCE SPECIFICATIONS

Parameter	Specification		
Number of Switching Ports	4-20		
Number of Express Ports (E)	7 – 9		
Number of Add/Drop Ports (A)	8 – 13		
Frequency Range: C Band	191.3 – 196.1 THz		
Channel Count	96 (50 GHz)		
Clear Passband	± 12 GHz for (50 GHz)		
Bandwidth: -0.5 dB	± 14 GHz		
Bandwidth: -3.0 dB	± 18 GHz		
Optical Specifications	**Typical**	**Maximum**	
Insertion Loss		6.5 dB (E)	7.5 dB (A)
Polarization Dependent Loss (PDL)	0.25 dB	0.85 dB (E)	0.90 dB (A)
Port Isolation (Channel Crosstalk)	≤ -40 dB	≤ -35 dB (E)	≤ -25 dB (A)
Block Extinction	≤ -40 dB	≤ -35 dB	
Attenuation Range		20 dB	
Attenuation Resolution		0.1 dB	
Attenuation Accuracy: 0 – 10 dB		± 1.0 dB	
Attenuation Accuracy: 10 – 15 dB		± 1.2 dB	
Module Specifications			
Dimensions	220 x 140 x 37 mm		
Communications Interface	DPRAM, serial		
Electrical Connector	CLP-140-02-S-D (Samtec)		
Power Consumption (typical)	20 W		

Fig 11.1. Finisar's WSS

12. References

[1] 3.07 Optical Communications Dan M. Marom, the Hebrew University of Jerusalem, Jerusalem, Israel.

[2] Sterling Perrin "Building a Fully Flexible Optical Layer with Next-Generation ROADMs

[3] Dan M. Marom, Member, IEEE, David T. Neilson, Senior Member, IEEE, Member, OSA, Dennis S. Greywall, Chien-Shing Pai, Nagesh R. Basavanhally, Vladimir A. Aksyuk, Daniel O. López, Flavio Pardo, Maria Elina Simon, Yee Low, Paul Kolodner, and Cristian A. Bolle "Wavelength-Selective 1× K Switches Using Free-Space Optics and MEMS Micro mirrors: Theory, Design, and Implementation" JOURNAL OF LIGHTWAVE TECHNOLOGY, VOL. 23, NO. 4, APRIL 2005

[4] C. Soutar and K. H. Lu, "Determination of the physical properties of an arbitrary twisted-nematic liquid crystal cell" Opt. Eng. 33 2704–12 (1994).

[5] A. Yariv, and P. Yeh, "Photonics: Optical Electronics in Modern Communications (Oxford University Press, New York, NY, 2006), 6th ed".

[6] David Sinefeld and Dan M. Marom, Senior Member, IEEE "Insertion Loss and Crosstalk Analysis of a Fiber Switch Based on a Pixelized Phase Modulator" JOURNAL OF LIGHTWAVE TECHNOLOGY, VOL. 29, NO. 1, JANUARY 1, 2011

[7] C. Palmer "Diffraction Grating Handbook - 5th Edition"

[8] Sinefeld, David; Ella, Roy; Zaharan, Ofer; Valiano, Yuval; Mach, Eliezer; Marom, Dan M "Adaptive Wavefront Aberration Correction in a Free-Space Fiber-Optic System based only on the Received Power" OSA/ CLEO 2011

[9] Zemax manual